
Clustering Aware Classification for Risk Prediction & Subtyping in Clinical Data

Shivin Srivastava¹ Siddharth Bhatia¹ Lingxiao Huang² Jun Heng Lim³ Kenji Kawaguchi¹ Vaibhav Rajan¹

¹School of Computing, National University of Singapore, Singapore

²Huawei TCS Labs, Shanghai, China

³Nanyang Institute of Technology, Singapore

Abstract

In data containing heterogeneous subpopulations, classification performance benefits from incorporating the knowledge of cluster structure in the classifier. Previous methods for such combined clustering and classification either 1) are classifier-specific and not generic, or 2) independently perform clustering and classifier training, which may not form clusters that can potentially benefit classifier performance. The question of how to perform clustering to improve the performance of classifiers trained on the clusters has received scant attention in previous literature, despite its importance in several real-world applications. In this paper, first, we theoretically analyze the generalization performance of classifiers trained on clustered data and find conditions under which clustering can potentially aid classification. This motivates the design of a simple k -means-based classification algorithm called **Clustering Aware Classification (CAC)** and its neural variant **DEEPCAC**. DEEPCAC effectively leverages deep representation learning to learn latent embeddings and finds clusters in a manner that make the clustered data suitable for training classifiers for each underlying subpopulation. Our experiments on synthetic and real benchmark datasets demonstrate the efficacy of DEEPCAC over previous methods for combined clustering and classification.

1 Introduction

Many real datasets have complex underlying structures such as clusters and intrinsic manifolds. For classification tasks

on such data, linear classifiers fail to learn well because of the inherent non-linear data distribution. Non-linear classifiers such as (deep) neural networks perform well in such cases, but often require large training data sets to achieve good generalization. When clusters are found or suspected in the data, it is well known that classification performance benefits from incorporating knowledge of such cluster structure in the model, for both linear and non-linear classifiers [1–4].

As an example, consider the problem of predicting the risk of disease using patients’ clinical data. Patient populations, even for a single disease, show significant clinical heterogeneity. As a result, subpopulations (called subtypes) having relatively homogeneous clinical characteristics can often be found in the data. Models that do not consider underlying subtypes may be consistently underestimating or overestimating the risks in specific subtypes [5], and risk models that account for subtypes are more effective [4, 6–8]. Similar examples illustrate the benefit of clustering to build classifiers in, e.g., image processing [9, 10] and natural language processing [11].

Previous works on using clustering for classification broadly fall into two categories. The first group of techniques modify specific classification techniques to account for the underlying clusters, e.g., Clustered SVMs [2]. These techniques are closely tied to the modified classifier and inherit both its modeling strengths and weaknesses. The second and more common approach is to first cluster the data and then independently train classifiers on each cluster. Although simple and intuitive, such a ‘cluster-then-predict’ approach is not designed to form clusters optimized to improve the performance of classifiers trained on those clusters. To the best of our knowledge, the question of performing clustering to improve the performance of classifiers trained on the clusters has not been addressed by previous literature.

Thus, in this paper, we first investigate the fundamental question of when and how clustering can help in obtaining accurate classifiers. Our analysis yields novel insights into the benefits of using simple classifiers trained on clusters compared to simple or complex (in terms of Rademacher

arXiv:2102.11872v5 [cs.LG] 3 Jan 2023

complexity [12]) classifiers trained without clustering. It provides clues on when such a clustering-based approach may or may not improve the subsequent classification. This leads to the design of our first clustering-based algorithm for classification, called Clustering Aware Classification (CAC). CAC finds clusters that are intended to be used as training datasets by the (base) classifiers of choice e.g., logistic regression, SVM, or neural networks. The key idea of our approach is to induce class separability (polarization) within each cluster, for better downstream classification, in addition to partitioning the data. This is effected by designing a cost function that can be used within the optimization framework of k -means.

Theoretical and empirical analysis of CAC demonstrates the benefits of inducing class separability in clusters for downstream classification. However, linear separability in CAC and clustering in the data space do not yield good quality clusters. To address this limitation we turn to recent deep clustering methods that have shown the efficacy of clustering on low-dimensional embeddings obtained from deep representation learning, through autoencoders. Adopting this approach for simultaneous clustering and classification is not straightforward as we face two hurdles. First, the class-separability loss in CAC cannot be optimized directly during network training. Second, we often obtain degenerate clustering solutions with empty clusters. We solve these two problems in our second algorithm DEEPCAC, a neural variant of CAC, that uses an additive margin softmax loss to induce class separability in clusters and a normalization term to avoid degenerate solutions. In summary, our contributions are:

1. Our theoretical analysis provides insights into the fundamental question of how clustering can aid in potentially improving the performance of classifiers trained on the clusters.
2. We propose the concept of class separation aware clustering and provide a theoretical result showing how class separation bounds the log-loss of clusters. We design a simple, proof-of-concept algorithm, Clustering Aware Classification (CAC) based on k -means algorithm. We conduct extensive empirical studies on synthetic data and real data to evaluate its efficacy and validate our theoretical results.
3. We propose DEEPCAC, a novel model for simultaneous clustering and classification that realizes cluster-specific class separation through additive margin softmax loss. We introduce novel techniques to stabilize training and prevent degenerate clusters.
4. Our experimental results on benchmark clinical datasets show that DEEPCAC yields improved performance over the state-of-art approaches for combined clustering and classification on large, highly imbalanced datasets while being comparable on mid-sized datasets. We also demonstrate the practical utility of our approach through a case study on the prediction of length of stay in Intensive Care Units in hospitals.

REPRODUCIBILITY: Our code and datasets are publicly available at [this anonymous link](#).

2 Related Work

The idea of training multiple local classifiers on portions of the dataset has been extensively studied for specific classifiers [13–20]. For instance, [21] presents a novel locality-sensitive support vector machine (LSSVM) for the image retrieval problem. Locally Linear SVM [22] has a smooth decision boundary and bounded curvature. Its authors show how functions defining the classifier can be approximated using any local coding scheme.

There are other related works, which aim to find suitable representations of raw data such that the performance in downstream prediction tasks is better when they use the learned embeddings. Large Margin Nearest Neighbour (LMNN) [23] introduces the much-celebrated triplet loss. In this work, the authors find a data-specific Mahalanobis distance embedding for the data, subject to the constraint that k similarly labeled points are mapped in the neighborhood of every point. The transformed data is more amenable for a k Nearest Neighbour classifier to work with. [24] extends LMNN to make it parameter-free. Some Bayesian approaches have been developed for combined classification and clustering, e.g., [1, 25] but they are computationally expensive.

Recent neural models for combined clustering and classification, that are closest to our work, are DMNN, GRASP and, AC-TPC. In Deep Mixture Neural Network (DMNN) [4] neural representations, from an encoder, are clustered using softmax gating and a mixture of experts, comprising neural networks, is used to predict risk. However, as seen in our experiments, clustering through softmax gating does not yield well-characterized subtypes and does not improve risk prediction. GRASP [26] aims to boost healthcare models by incorporating auxiliary information from similar patients. In GRASP, clustering and prediction processes influence and enhance each other over iterations and thus it can be viewed as an algorithm for simultaneous classification and clustering. In [27] an Actor-Critic Approach for Temporal Predictive Clustering (AC-TPC) is designed wherein latent representations from patient data are clustered ensuring intra-cluster homogeneity in outcomes. A predictor neural network is conditioned on cluster centroids, with actor-critic training.

3 Background

Given a set of data samples $X = (x_1, x_2, \dots, x_N)$ with N records $x_i \in \mathbb{R}^d$ together with binary labels $y_i \in \{0, 1\}$, the task of clustering is to group the N points into K clusters. K -means is arguably the most widely adopted algorithm due to its simplicity, speed, properties that are well studied in literature [28, 29]. It works by optimizing the following

cost function:

$$\min_{M \in \mathbb{R}^{M \times K}, \{s_i \in \mathbb{R}^K\}} \sum_{i=1}^N \|x_i - M s_i\|_2^2$$

s.t. $s_{j,i} \in \{0, 1\}, \mathbf{1}^T s_i = 1 \quad \forall i, j$

where s_i is the assignment vector of data point i which has only one non-zero element, $s_{j,i}$ denotes the j^{th} element of s_i , and the k^{th} column of M (the cluster assignment matrix), i.e., m_k , denotes the centroid of the k^{th} cluster. k -means works well when the data points are evenly distributed about their centroids. Real world data, however, are generally high dimensional and thus not ‘ k -means friendly’. The Deep Clustering Network (DCN) [30] algorithm solves this problem by designing a deep neural network (DNN) structure and the associated joint optimization criterion for joint dimensionality reduction (DR) and clustering instead of using DR as a mere preprocessing technique, also followed in other works, e.g. [31, 32]. The loss function they optimize takes the form:

$$\min_{\mathcal{U}, \mathcal{W}} \ell(X, g(f(X))) + \beta \cdot \sum_{i=1}^N \|f(x_i) - M s_i\|^2 + \gamma \cdot r(f(X))$$

where $X = [x_1, \dots, x_N]$, $\beta > 0$ is a parameter for balancing data fidelity and the latent cluster structure; ℓ is a function that measures the reconstruction error. Popular choices for ℓ include the KL divergence loss and least square loss; r is a regularization imposed upon the latent embeddings to encourage other properties (like class separability in our case) weighted by $\gamma > 0$.

4 Problem Statement

Let $X = (x_1, x_2, \dots, x_N)$ be a training dataset with N records $x_i \in \mathbb{R}^d$ together with binary labels $y_i \in \{0, 1\}$. Given an integer $k \geq 1$, our goal is to:

1. Divide X into k non-empty, distinct clusters $\mathcal{C} = \{C_1, C_2, \dots, C_k\}$, and
2. Obtain a collection of k classifiers $\mathcal{F} = \{f_1, f_2, \dots, f_k\}$ where each $f_j : C_j \rightarrow \{0, 1\}^{|C_j|}$ is trained on all $x_i \in C_j$ with the objective $\arg\min_{\mathcal{F}, \mathcal{C}} \sum_{j=1}^k \sum_{i \in C_j} \ell(f_j(x_i), y_i)$.

There is no restriction on the choice of the classifier, which is determined apriori by the user.

5 Can Clustering Aid Classification?

We provide a principled motivation behind our clustering approach by analyzing when clustering can potentially help obtain accurate classifiers. Our analysis yields

crucial insights into developing the CAC framework. Fix $j \in \{1, \dots, k\}$ and let $S_j = \{(x_i, y_i)\}_{i=1}^{m_j}$ be the training dataset from the j -th cluster (having m_j points) with $x \in \mathcal{X}_j$ and $y \in \mathcal{Y}_j$ s.t. $\mathcal{X}_j = \{x : x \in C_j\}$ and $\mathcal{Y}_j = \{y : y \in C_j\}$. Then, the following theorem — a direct application of a previous result [12, 33] to our problem — suggests a potential benefit of clustering in terms of the expected error $\mathbb{E}_{x,y}[\ell(f(x), y)]$ for unseen data:

Theorem 1 (Proof in Appendix 11.1). *Let \mathcal{F}_j be a set of maps $x \in C_j \mapsto f_j(x)$. Let $\mathcal{F} = \{x \mapsto f(x) : f(x) = \sum_{j=1}^K \mathbb{1}\{x \in C_j\} f_j(x), f_j \in \mathcal{F}_j\}$. Suppose that $0 \leq \ell(q, y) \leq \lambda_j$ for any $q \in \{f(x) : f \in \mathcal{F}_j, x \in C_j\}$ and $y \in \mathcal{Y}_j$. Then, for any $\delta > 0$, with probability at least $1 - \delta$, the following holds: for all maps $f \in \mathcal{F}$,*

$$\mathbb{E}_{x,y}[\ell(f(x), y)] \leq \sum_{j=1}^K \Pr(x \in C_j) \cdot \left(\frac{1}{m_j} \sum_{i=1}^{m_j} \ell(f(x_i^j), y_i^j) + 2\hat{\mathcal{R}}_{m_j}(\ell \circ \mathcal{F}_j) + 3\lambda_j \sqrt{\frac{\ln(K/\delta)}{2m_j}} \right), \quad (1)$$

where

$$\hat{\mathcal{R}}_{m_j}(\ell \circ \mathcal{F}_j) := \mathbb{E}_{\sigma}[\sup_{f_j \in \mathcal{F}_j} \frac{1}{m_j} \sum_{i=1}^{m_j} \sigma_i \ell(f_j(x_i), y_i)],$$

$\Pr(x \in C_j) = 1$ if $x \in C_j$ and $\sigma_1, \dots, \sigma_{m_j}$ are independent uniform random variables taking values in $\{-1, 1\}$.

Theorem 1 shows that the expected error $\mathbb{E}_{x,y}[\ell(f(x), y)]$ for unseen data is bounded by three terms: the training error $\frac{1}{m_j} \sum_{i=1}^{m_j} \ell(f(x_i), y_i)$, the Rademacher complexity $\mathcal{R}_{m_j}(\ell \circ \mathcal{F}_j)$ of the set of classifiers \mathcal{F}_j on the j -th cluster, and the last term $O(\ln(K/\delta)/2m_j)$ in equation (1). To apply Theorem 1 to models without clustering, we can set the j -th cluster to contain all data points with $m_j = N$.

The upper bound can be used to analyze the benefit of using a simple model (e.g., a linear model) *with* clustering compared to two cases of (1) a simple model and (2) a complex model (e.g., a deep neural network), both *without* clustering. For a simple model *without* clustering, the training error term $\frac{1}{m_j} \sum_{i=1}^{m_j} \ell(f(x_i^j), y_i^j)$ in equation (1) can be large, because a simple model may not be able to sufficiently separate training data points (underfitting) to minimize the training error. In the case of a complex model *without* clustering, the training error can be small but the Rademacher complexity $\mathcal{R}_{m_j}(\ell \circ \mathcal{F}_j)$ tends to be large. A simple model *with* clustering can potentially trade-off these by minimizing Rademacher complexity $\mathcal{R}_{m_j}(\ell \circ \mathcal{F}_j)$ while making the training data in the cluster linearly separable to minimize training error $\frac{1}{m_j} \sum_{i=1}^{m_j} \ell(f(x_i^j), y_i^j)$. This observation leads us to explore ways to induce class separability in data clusters.

6 CAC

The previous section discusses factors that give us hints of possible scenarios when clustering can aid classification.

Using a simple model with clustering can be potentially advantageous when the first and second terms in the RHS of Equation (1) are dominant. It thus motivates the formation of clusters, each of which can be linearly separable internally with respect to the classes for further improved performance of downstream simple classifiers. We test our idea by designing a simple algorithm, Clustering Aware Classification (CAC), that finds clusters to be used as training datasets by a chosen classifier. The key idea is to induce class separability within clusters to aid downstream cluster-specific classifiers. During clustering, we measure the class separability by developing a metric based on class-specific centroids within each cluster, and theoretically analyze the effect of its use on the classification error.

Class Separability: We use a simple heuristic to measure class separability within each cluster. For each cluster C_j ($j \in [k]$), we define: *cluster centroid*: $\mu(C_j) := |C_j|^{-1} \sum_{x_i \in C_j} x_i$, *positive centroid*: $\mu^+(C_j) := (\sum_{x_i \in C_j} y_i)^{-1} \sum_{x_i \in C_j} y_i x_i$, and *negative centroid*: $\mu^-(C_j) := (\sum_{x_i \in C_j} (1 - y_i))^{-1} \sum_{x_i \in C_j} (1 - y_i) x_i$. Class separability is defined as the distance between positive and negative centroids within each cluster i.e. $\|\mu^+ - \mu^-\|$.

Bounding Log-Loss of Classifiers in terms of Class Separation: We now show how class separation within clusters has a direct effect on the training error of classifiers employing log-loss. The following theorem also validates our choice of using $\|\mu^+ - \mu^-\|$ as a heuristic to measure class separability.

Theorem 2 (Proof in Appendix 11.3). *Let $X = (x_1, x_2, \dots, x_N)$ be a training dataset with N records $x_i \in \mathbb{R}^d$ together with binary labels $y_i \in \{0, 1\}$. Define the log-loss over the entire dataset as: $\ell(X) = -\sum_i y_i \ln(p(x_i)) + (1 - y_i) \ln(1 - p(x_i))$, where $p(x_i) = [1 + \exp(-\beta x_i)]^{-1}$ and $\beta = \operatorname{argmin}_\beta \ell(X)$. Then,*

$$C_1 - (C_3 \beta \mu^+ - C_4 \beta \mu^-) \leq \ell(X) \leq C_2 - (C_3 \beta \mu^+ - C_4 \beta \mu^-)$$

where $C_1 = N \ln(2)$, $C_2 = N \ln(1 + \exp(c)) - \frac{Nc}{2}$, $C_3 = \frac{N^+}{2}$, $C_4 = \frac{N^-}{2}$, $N^+ = \sum_{x_i \in X} y_i$, $N^- = \sum_{x_i \in X} (1 - y_i)$ and $c = \operatorname{argmax}_i \|\beta x_i\|$.

Clusters with Class Separability: To induce our notion of class separability within clustering we consider the k -means clustering formulation that is widely used for its simplicity, effectiveness, and speed. Clusters using k -means are obtained by minimizing the size-weighted sample variance of each cluster: $\mathcal{D}(X) = \sum_{p=1}^k \inf_{\mu(C_p) \in X} \sum_{i \in C_p} \|x_i - \mu(C_p)\|^2$. To induce class separability, a natural formulation is to add a cost with respect to class separability for each cluster. With our measure for class separability, and $\alpha > 0$ as a class separation hyperparameter, we get $\phi(C_j) = \sum_{i \in C_j} (\|x_i - \mu(C_j)\|^2 - \alpha \cdot \|\mu^+(C_j) - \mu^-(C_j)\|^2)$.

Defining the cost function in this manner encourages the decrease of cluster variance term and increase of the class separability term, weighted by α . Consequently, the overall cost function defined as $\phi(\{C_j\}_1^k) := \sum_{j=1}^k \phi(C_j)$ and the CAC algorithm aims to minimize that. We optimize for $\phi(\{C_j\}_1^k)$ by using the Hartigan’s method [34] instead of the more common Lloyd’s Algorithm [28]. Our approach is summarized in Algorithm 1. $\Phi(x_i; C_p, C_q)$ represents the overall decrease in the cost function for the entire dataset if the point x_i is moved from cluster C_p to C_q (see Appendix 10 for more details).

In conclusion, Theorem 2 points out that under certain conditions (See Lemma 2 in Appendix 11.2), the upper and lower bounds of log-loss provably decrease. The gap between the upper and lower bounds is a direct function of the breadth of the cluster. Thus as clusters become tighter, the training log-loss of the classifiers becomes more tightly bound. Classification results on real datasets (see Table 5 in Appendix) show that CAC outperforms the simple cluster-then-predict approach on multiple base classifiers.

We however note that CAC has several limitations. Firstly, CAC assumes linear class separability which is not a realistic assumption in real world data. Moreover, the restriction of working in the original data space leads to poor quality of clusters as compared to those found by plain k -means (c.f. Fig. 5 in Appendix). CAC initialized with k -means has a good Silhouette Index which decreases with training iterations). We thus turn to representation learning to discover transformations that conform to requirements of class separability and clustering while not being brittle at the same time. This motivates the design of the neural variant of CAC, DEEPCAC, which addresses these limitations by clustering in a low-dimensional embedding space instead of the data space, where the embeddings are obtained via non-linear dimensional reduction algorithms like deep autoencoders.

7 DEEPCAC

Network Architecture: We propose to employ a Stacked Autoencoder (SAE) for dimensionality reduction. Figure 2 illustrates the DEEPCAC architecture. An SAE consists of an encoder (E) and decoder (D) parameterized by $(\mathcal{U}, \mathcal{V})$ as $E(\mathcal{U}) : X \rightarrow Z$ and $D(\mathcal{V}) : Z \rightarrow X$. The encoder transforms the raw data into the embedded data space Z (or the ‘bottleneck’ layer). The ‘decoding’ layers that try to reconstruct the data from the latent space are on the right-hand side. In the subsequent classification stage after the clustering stage, there exist k local networks $(\{LN_j(\mathcal{W}_j)\}_{j=1}^k)$ that are trained separately from the autoencoder. Similar to CAC, the data points are clustered but now in the embedded data space Z . Note that, unlike cluster-then-predict approaches, clustering is not independent of classification since class labels are used during clustering as described below.

Algorithm 1: CAC

Input: Training Data: $X \in \mathbb{R}^{N \times d}$, binary labels $y^{n \times 1} \in \{0, 1\}^N$, $\{C_j\}_1^k$, $\{f_j\}_1^k$ and α

- 1 \triangleright **Initialization**
- 2 Compute $\mu(C_j), \mu^+(C_j), \mu^-(C_j) \forall C_j$ s.t. $j \in \{1, \dots, k\}$.
- 3 \triangleright **Algorithm**
- 4 **while not converged do**
- 5 **for** $i \in \{1 \dots N\}$ **do**
- 6 **if** Removing $x_i \in C_p$ from its cluster does not lead to a 1-class cluster **then**
- 7 \triangleright **Assign new cluster to** x_i
- 8 Let $q := \operatorname{argmin}_j \Phi(x_i; C_p, C_j)$ (breaking ties arbitrarily).
- 9 **if** $\Phi(x_i, C_p, C_q) < 0$ **then**
- 10 Assign x_i to C_q from C_p and update $\mu(C_p), \mu(C_q), \mu^\pm(C_p)$ and $\mu^\pm(C_q)$.
- 11 **Otherwise**, let x_i remain in C_p .
- 12 \triangleright **Train Classifiers**
- 13 For every cluster C_j , train a classifier f_j on $(\mathcal{X}_j, \mathcal{Y}_j)$.
- 14 **Output** Classifiers $\mathcal{F} = \{f_j\}_{j=1}^k$ and cluster centroids $\mu = \{\mu_j\}_{j=1}^k$

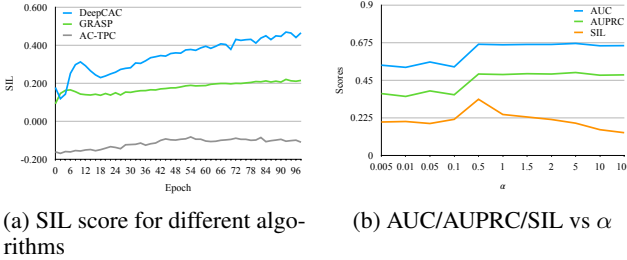


Figure 1: (a) Silhouette scores vs. epochs. (b) Sensitivity Analysis with AUC/AUPRC and Silhouette scores (on DEEPCAC) on CIC dataset. $k = 3$ in all experiments.

Loss Function: The DEEPCAC loss function consists of 3 parts: The auto-encoder reconstruction error term ($\|x_i - D(E(x_i))\|^2$) that regularizes the encoder as suggested by [35]. The sum of squared errors (SSE) term ($\frac{\|E(x_i) - Ms_i\|^2}{|C_j| - 1 + \delta}$) that encourages points to lie close to their cluster centroid thus forming k -means friendly clusters, and a third term that we explain in the next paragraph. Unlike previous approaches [36] that employ ad-hoc methods like cluster resampling in the case of an empty cluster, we normalize the cluster SSE (dividing it by the size of cluster) to stabilize training and prevent degenerate solutions.

The CAC loss function encourages cluster structure formation and intra-cluster class separation by directly optimizing

for the distance between class cluster centroids. The class separation term in CAC encourages a gap between individual class points in respective clusters. But we observed that DEEPCAC was not able to directly optimize such a formulation of class separability through gradient descent. So we replace the CAC class separation term with the well-known Additive Margin Softmax Loss (AM Softmax) [37] as another way of inducing class separability within clusters. The AM Softmax loss includes an additive margin to the standard softmax loss to push the classification boundary closer to the weight vector of each class. The final loss function of DEEPCAC thus becomes:

$$L = \sum_{j=1}^k \sum_{i \in C_j} \|x_i - D(E(x_i))\|^2 + \frac{\beta * \|E(x_i) - Ms_i\|^2}{|C_j| - 1 + \delta} - \frac{\alpha}{|C_j|} \sum_i \log \frac{e^{s \cdot (W_{y_i}^T z_i - m)}}{e^{s \cdot (W_{y_i}^T z_i - m)} + \sum_{j=1, j \neq y_i}^c e^{s W_j^T z_i}} \quad (2)$$

s.t. $s_{j,i} \in \{0, 1\}, \mathbf{1}^T s_i = 1 \forall i, j$

where W_j^T is the j -th column of the last fully connected layer of the AMSoftmax loss. M denotes the centroid matrix and $s_{i,j}$ is the assignment vector of data point x_i which has only one non-zero element. $s_{j,i}$ denotes the j^{th} element of s_i . μ_k , the k^{th} column of M , denotes the centroid of the k^{th} cluster, z_i is the embedding for x_i and $|C_j|$ is the cardinality of cluster C_j .

How does AM Softmax loss induce class separability?

Theorem 3 (Proof in Appendix 11.4). *Let $X = (x_1, x_2, \dots, x_N)$ be a training dataset with N records $x_i \in \mathbb{R}^d$ together with binary labels $y_i \in \{0, 1\}$. Define the AM Softmax loss over the entire dataset as :*

$$-\sum_i \log \frac{e^{s \cdot (w_{y_i}^T z_i - m)}}{e^{s \cdot (w_{y_i}^T z_i - m)} + \sum_{j=1, j \neq y_i}^c e^{s W_j^T z_i}}. \text{ Then,}$$

$$K_1 - \Gamma(K_3 \mu^+ - K_4 \mu^-) \leq L_{AMS}(X) \leq K_2 - \Gamma(K_3 \mu^+ - K_4 \mu^-)$$

where $K_1 = N \left(\log 2 + \frac{sm}{2} \right)$, $K_2 = N(1 + sm)$, $K_3 = sN^+$, $K_4 = sN^-$, $N^+ = \sum_{x_i \in X} y_i$, $N^- = \sum_{x_i \in X} (1 - y_i)$ and $\Gamma = W_+^T - W_-^T$.

The upper and lower bounds for the AM-softmax loss are strikingly similar to those of the logistic loss found in theorem 2. We note that as L_{AMS} decreases, it pushes the lower bound to become smaller. The agent vectors ($W_{+/-}$) will lie nearby the class centroids ($\mu^{+/-}$) [38] and can thus be approximated as $W_+ \sim \mu^+$ and $W_- \sim \mu^-$. The lower bound for L_{AMS} can then be simplified as $K_1 - \Gamma(K_3 \mu^+ - K_4 \mu^-) = K_1 - sN(1 - \mu^+ \cdot \mu^-)$ (since $|\mu^+| = |\mu^-| = 1$). This implies that as L_{AMS} pushes down the lower bound, $\mu^+ \cdot \mu^-$ must decrease i.e. class centroids move further away (separate) from each other on the L_2 hypersphere. From

theorem 2, we know that an increasing class separation decreases the training log-loss. Thus replacing CAC loss with the AM-Softmax loss achieves the same purpose.

Training: DEEPCAC is trained in 3 stages: (i) Pre-training, (ii) Training the clustering network and (iii) Training the local networks. During pre-training the autoencoder parameters $(\mathcal{U}, \mathcal{V})$ are initialized by training the autoencoder to minimize the reconstruction loss without activating the DEEPCAC loss functions. Once the autoencoder is initialized, the data embeddings are clustered using the k -means algorithm and the cluster centroids are initialized. The overall DEEPCAC loss function is non-convex and difficult to optimize. Stochastic gradient descent (SGD) cannot be directly applied to jointly optimize $\mathcal{U}, \mathcal{V}, M$, and $\{s_i\}$ because the block variable $\{s_i\}$ is constrained on a discrete set. We thus use an alternating scheme, similar to [30], to optimize the subproblems w.r.t. one of $M, \{s_i\}$ and $(\mathcal{U}, \mathcal{V})$ while keeping the other two sets of variables fixed. Further details regarding the updating of network parameters can be found in Appendix 12. Finally, the local networks are trained on the clusters found by the encoder in the representation space. Algorithm 2 summarizes the entire procedure.

Algorithm 2: DEEPCAC

Input: Training Data: $X \in \mathbb{R}^{n \times d}$, class labels $y^{n \times 1} \in [\mathcal{B}]^n, \{C_j\}_1^k, \{f_j\}_1^k$

- 1 \triangleright **Initialization**
- 2 Pretrain E and D to initialize \mathcal{U}, \mathcal{V}
- 3 Compute $\mu(C_j) \forall C_j$ s.t. $j \in \{1, \dots, k\}$.
- 4 \triangleright **Algorithm**
- 5 **while not converged do**
- 6 **for every mini-batch \mathcal{X}_b do**
- 7 Update Network parameters by backpropagating L (Eq. 2)
- 8 Update cluster assignments
- 9 Update cluster centroids
- 10 \triangleright **Train Classifiers**
- 11 $\mathcal{Z} \leftarrow E(\mathcal{X})$
- 12 For every cluster C_j , train a classifier f_j on $(\mathcal{Z}_j, \mathcal{Y}_j)$.
- 13 **Output Output** Trained Network E and cluster centroids $\mu = \{\mu_j\}_{j=1}^k$ in embedded space.

8 Experiments

We perform two sets of experiments. The first set of experiments, on synthetic data, studies the sensitivity of CAC on various characteristics of the data like cluster separation and class separation within clusters. We find that cluster-then-predict method does enhance overall classifier performance and exploiting class separation can lead to further improvements. Appendix 11.8 presents the details

of these experiments and the results. In the second set of experiments, described below, we compare the performance of CAC with that of other methods on real benchmark datasets.

Table 1: Dataset Summary. MAJ: proportion of majority class.

Dataset	#Instances	#Features	MAJ
Sepsis [39]	30661	209	0.07
WID Mortality [40]	91711	241	0.91
Diabetes [41]	100000	9	0.41
Respiratory [42]	22450	486	0.92
CIC [43]	12000	117	0.85
CIC-LOS	12000	116	–

Real Datasets: We evaluate CAC and DEEPCAC on 6 clinical datasets (Table 1). CIC refers to the dataset from the 2012 Physionet challenge [44] to predict in-hospital mortality of intensive care unit (ICU) patients at the end of their hospital stay. The dataset has time-series records, comprising various physiological parameters, of 12,000 patient ICU stays. We follow the data processing scheme of [43] (the top-ranked team in the competition) to obtain a static 117-dimensional feature vector for each patient. The Sepsis dataset is derived from the 2019 Physionet challenge of sepsis onset prediction. It has time series records, comprising various physiological parameters of ~ 40000 patients. We follow the data processing scheme of the competition winners [45] to obtain static 89 dimensional features for each patient. WID data is from the Women In Data Science challenge [40] to predict patient mortality. The Diabetes dataset is from the UCI Repository where the task is to predict patient readmission. The Respiratory data has been extracted by us for the tasks of Acute Respiratory Distress Syndrome (ARDS) prediction. For the Sepsis and ARDS datasets, we use the first, last, median, minimum, and maximum values in the first 24 hours as features for the temporal variables. The final feature vector dimensions for ARDS and Sepsis data are 486 and 209 respectively. All the above tasks are posed as binary classification problems. We also derive a multiclass dataset (CIC-LOS) from the CIC dataset where we predict the Length of Stay (LOS), discretized into 3 classes (based on 3 quartiles).

Experimental Setup: We evaluate the performance of CAC with a cluster-then-predict approach where k -means is used to cluster and multiple classifiers are used. We also compare its performance with that of the classifier directly, where no clustering is used. These are evaluated on a held-out test split comprising 25% of the data. DEEPCAC and its baselines are evaluated on 5 random train-validation-test splits for each dataset in the ratio 57-18-25 (Test data is 25% of the entire dataset and the validation dataset is 25% of the remaining data). Standard binary classification metric, the AUPRC (Area Under Precision-Recall curve) score is used to evaluate classifier performance, as there is an imbalance in many datasets. All models are trained until the AUPRC

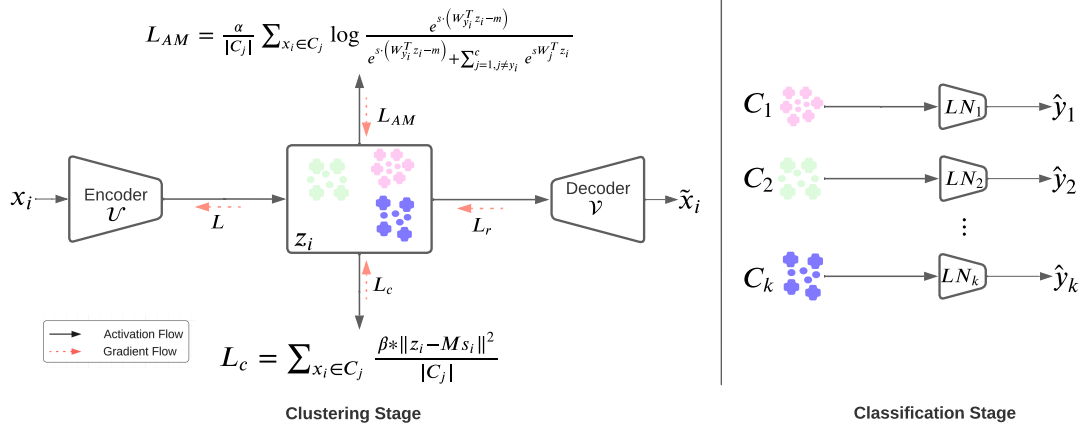


Figure 2: In the clustering stage an encoder is trained to find representations that are clustered with good class separability. In the classification stage, cluster-specific classifiers are trained on the representations. L_{AM} and L_C are defined in eqn. 2.

Table 2: AUPRC of DEEPCAC and other baselines. Best values in **bold**. Following KM, DCN, and IDEC, we use the same local classifier (denoted by -Z) that is used by DEEPCAC. AUC values, that show a similar trend, are shown in Appendix 13.

Dataset	k	KM-Z	DCN-Z (2017)	IDEC-Z (2017)	DMNN (2020)	AC-TPC (2020)	GRASP (2021)	DEEPCAC (Ours)
Diabetes	2	0.528 ± 0.011	0.556 ± 0.002	0.553 ± 0.007	0.53 ± 0.005	–	0.538 ± 0.007	0.558 ± 0.004
	3	0.514 ± 0.016	0.556 ± 0.003	0.548 ± 0.01	0.539 ± 0.007	0.523 ± 0.0	0.542 ± 0.007	0.56 ± 0.002
	4	0.507 ± 0.02	0.556 ± 0.003	0.553 ± 0.005	0.536 ± 0.004	0.5 ± 0.0	0.544 ± 0.008	0.555 ± 0.006
CIC	2	0.568 ± 0.014	0.609 ± 0.036	0.674 ± 0.036	0.636 ± 0.03	–	0.757 ± 0.036	0.753 ± 0.023
	3	0.527 ± 0.028	0.612 ± 0.017	0.587 ± 0.032	0.667 ± 0.016	0.656 ± 0.0	0.755 ± 0.039	0.746 ± 0.018
	4	0.54 ± 0.033	0.594 ± 0.025	0.618 ± 0.016	0.636 ± 0.025	0.663 ± 0.0	0.743 ± 0.031	0.743 ± 0.014
CIC-LoS	2	0.396 ± 0.008	0.44 ± 0.02	0.452 ± 0.013	0.429 ± 0.007	–	0.478 ± 0.021	0.485 ± 0.004
	3	0.353 ± 0.019	0.425 ± 0.022	0.406 ± 0.029	0.435 ± 0.013	0.426 ± 0.0	0.473 ± 0.026	0.488 ± 0.008
	4	0.344 ± 0.018	0.443 ± 0.025	0.437 ± 0.014	0.429 ± 0.007	0.402 ± 0.0	0.474 ± 0.018	0.487 ± 0.006
ARDS	2	0.552 ± 0.023	0.563 ± 0.031	0.601 ± 0.009	0.536 ± 0.017	–	0.493 ± 0.004	0.604 ± 0.013
	3	0.527 ± 0.022	0.582 ± 0.017	0.565 ± 0.025	0.525 ± 0.012	0.553 ± 0.004	0.492 ± 0.004	0.594 ± 0.014
	4	0.503 ± 0.015	0.533 ± 0.03	0.588 ± 0.008	0.551 ± 0.016	0.55 ± 0.015	0.569 ± 0.069	0.592 ± 0.029
Sepsis	2	0.532 ± 0.014	0.595 ± 0.023	0.597 ± 0.021	0.539 ± 0.003	–	0.5 ± 0.005	0.646 ± 0.037
	3	0.515 ± 0.019	0.593 ± 0.017	0.596 ± 0.012	0.531 ± 0.012	0.579 ± 0.013	0.496 ± 0.001	0.654 ± 0.031
	4	0.517 ± 0.012	0.553 ± 0.029	0.601 ± 0.011	0.531 ± 0.018	0.574 ± 0.02	0.499 ± 0.002	0.628 ± 0.02
WID-M	2	0.645 ± 0.026	0.71 ± 0.029	0.69 ± 0.061	0.597 ± 0.013	–	0.702 ± 0.023	0.723 ± 0.015
	3	0.565 ± 0.037	0.679 ± 0.053	0.666 ± 0.062	0.583 ± 0.014	0.596 ± 0.0	0.698 ± 0.021	0.721 ± 0.011
	4	0.535 ± 0.044	0.664 ± 0.048	0.677 ± 0.049	0.593 ± 0.014	0.619 ± 0.0	0.681 ± 0.014	0.714 ± 0.021

score on the validation data set plateaus. The Area under the ROC Curve (AUC) is also reported in Appendix 13, Table 6.

Baselines: For evaluating CAC, we consider 9 classical base classifiers (X), both linear and nonlinear and report results of X, KM+X, and CAC+X. These are LR, Linear SVM, XGBoost (#estimators = 10), Linear Discriminant Analysis (LDA), single Perceptron, Random Forest (#trees = 10), k Nearest Neighbors ($k = 5$), SGD classifier and Ridge classifier (Ridge regressor predicting over the range $[-1, 1]$).

For evaluating DEEPCAC, we use two kinds of baselines. The first set has classifiers that employ a simple cluster-then-predict kind of method where clustering is independently performed first and classifiers are trained on each cluster (denoted by -Z). We compare with 3 clustering methods k -means (where we use an autoencoder to get embeddings

which are then clustered using k -means), Deep Clustering Network DCN [30], Improved Deep Embedded Clustering (IDEC) [35] and DMNN [46]. The second set of baselines includes methods where clustering and classification happen simultaneously. We compare DEEPCAC with GRASP [26] modified to use the same backbone model i.e. the encoder. We also compare with AC-TPC [27] which uses an actor-critic model to refine clusters depending on the feedback from the classification process.

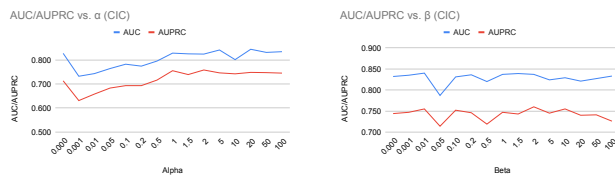
Hyperparameters: For DMNN and DEEPCAC, the autoencoder has 3 layers of sizes $64 - 32 - 64$ and a two-layer local predictor network of size $30 - 1$. The local prediction networks use Softmax and ReLU activation functions and are not regularized. The hyperparameters for deep learning methods, KM-Z, DCN-Z ($\beta = 2$), IDEC-Z

($\beta = 0.5$) and DEEPCAC ($\beta = 20, \alpha = 5$) are selected by conducting a sensitivity analysis (see Fig. 1) on the training set of the CIC-LoS dataset. For GRASP and AC-TPC, we use the hyperparameters suggested by the authors found using sensitivity analysis. The learning rate for DEEPCAC is set to $2e - 3$. The predictor, selector and encoder networks in AC-TPC are FCNs with $64 - 64$, $64 - 64$, and $32 - 32$ neurons respectively.

Results: The results for CAC are presented in Table 5 (Appendix 11.9) that summarises the F1 scores of CAC and baselines evaluated in clinical data sets. This is in line with Theorem 1 which predicts the better performance of multiple simple classifiers compared to a single simple classifier. We also observe that CAC performs better than the simple k -means + classification approach on 20 out of 27 (74%) experiments. This also serves as ablative evidence of the contribution of linear separability criteria since removing the latter reduces CAC to applying k -means and then predicting.

Table 2 presents the AUPRC scores obtained by DEEPCAC and its baselines. DEEPCAC is consistently better than the simple combined clustering and classification (cluster-then-predict) baselines i.e., DMNN, KM-Z, DCN-Z, and IDEC-Z. This shows that classification aware clustering is necessary, as done by GRASP and DEEPCAC, to ensure good downstream classification performance. GRASP and DEEPCAC perform comparably on the CIC (moderately sized) dataset.² DEEPCAC outperforms GRASP by a significant margin on the rest of the datasets (the larger and more imbalanced datasets) for different number of clusters. Similar performance improvements are also observed when AUC is used as a metric (in Appendix 13). The code for AC-TPC (provided by the authors) did not run for $k = 2$ on all datasets. Figure 1 and 5 show how the clustering performance of DEEPCAC does not deteriorate with increasing epochs as compared to CAC.

Case Study: To show the practical clinical applicability of DEEPCAC we present a case study in Appendix 14 on length of stay prediction. As expected, we see that inferred clusters have differences in risk factors tailored to each subpopulation.



(a) AUC/AUPRC vs α on CIC (b) AUC/AUPRC vs β on CIC

Figure 3: Sensitivity Analysis and Ablation Study for DEEPCAC w.r.t. α and β hyperparameters for $k = 3$

Table 3: AUPRC Scores for Time series datasets. Row-wise best result in bold. AC-TPC did not finish execution in time.

AUPRC	k	GRASP-TS	DEEPCAC-TS
ARDS-TS	2	0.498	0.615
ARDS-TS	3	0.506	0.605
ARDS-TS	4	0.5	0.565
Sepsis-TS	2	0.501	0.704
Sepsis-TS	3	0.507	0.672
Sepsis-TS	4	0.495	0.648

Ablation Study and Sensitivity Analysis: We study the effect of α and β hyperparameters on the classification performance of DEEPCAC by varying them on the range $[0.0, 100]$ (see Fig. 3). Both AUC and AUPRC scores fall sharply as α is increased from 0 but they eventually increase, plateauing after $\alpha = 5$. The classification performance does not vary much with β . A value of 0 leads to the removal of the loss term; better results are obtained with non-zero values indicating that both loss terms contribute to performance.

Extending DEEPCAC for Other Data Modalities:

DEEPCAC can be easily extended for other input data modalities such as images, text and time series by modifying the encoder and decoder appropriately. We demonstrate one such case by using an LSTM-based AE for time series data (see Appendix 15 for more details). We evaluate all algorithms on the ARDS and Sepsis datasets as mentioned in table 1. We use the first 24 hours of data to predict risk (of each condition, separately) in the remaining ICU stay, which is aligned with a hospital-centric schedule for prediction. Our experimental evaluation shows that DEEPCAC outperforms similar extensions of GRASP. As expected, DEEPCAC-TS also performs better than DEEPCAC on the non time series versions of ARDS and Sepsis datasets.

9 Conclusion

In this paper, we theoretically analyze potential reasons for the good performance of classifiers trained on underlying clusters in data. Our analysis yields insights into the benefits of using simple classifiers trained on clusters compared to simple or complex classifiers trained without clustering. We use our analysis to develop a simple prototype algorithm, CAC, that enforces class separability within each group during cluster discovery. Empirical and theoretical analysis of CAC further illuminates reasons for clustering aiding classification. To further improve clustering in such settings, we combine the benefits of deep representation learning and CAC in our algorithm DEEPCAC. We use novel techniques to stabilize training and induce class separability within clusters in DEEPCAC. Experiments on clinical benchmark datasets demonstrate the efficacy of DEEPCAC

in classification and clustering. A limitation of DEEPCAC is that the hard definition of point clusters forces the local classifiers to treat interior and fringe points equally. This can lead to a loss in predictive performance and can be addressed in the future.

References

- [1] Qiang Qian, Songcan Chen, and Weiling Cai. Simultaneous clustering and classification over cluster structure representation. *Pattern Recognit.*, 45:2227–2236, 2012.
- [2] Quanquan Gu and Jiawei Han. Clustered support vector machines. In *AISTATS*, 2013.
- [3] Tanmoy Chakraborty. Ec3: Combining clustering and classification for ensemble learning. *2017 IEEE International Conference on Data Mining (ICDM)*, pages 781–786, 2017.
- [4] Xiangrui Li, D. Zhu, and Phillip D. Levy. Predicting clinical outcomes with patient stratification via deep mixture neural networks. *AMIA Joint Summits on Translational Science proceedings. AMIA Joint Summits on Translational Science*, 2020:367–376, 2020.
- [5] Ralph Snyderman. Personalized health care: From theory to practice. *Biotechnology Journal*, 7, 2012.
- [6] Ahmed M. Alaa, Jinsung Yoon, Scott Hu, and Mihaela van der Schaar. Personalized risk scoring for critical care patients using mixtures of gaussian process experts. *ArXiv*, abs/1605.00959, 2016.
- [7] Harini Suresh, Jen J. Gong, and John V. Guttag. Learning tasks for multitask learning: Heterogenous patient populations in the icu. *Proceedings of the 24th ACM SIGKDD International Conference on Knowledge Discovery & Data Mining*, 2018.
- [8] Zina M. Ibrahim, Honghan Wu, Ahmed A. Hamoud, Lukas Stappen, Richard J. B. Dobson, and Andrea Agarossi. On classifying sepsis heterogeneity in the icu: insight using machine learning. *Journal of the American Medical Informatics Association : JAMIA*, 27:437 – 443, 2020.
- [9] Tae-Kyun Kim and Roberto Cipolla. Mcboost: Multiple classifier boosting for perceptual co-clustering of images and visual features. In *NIPS*, 2008.
- [10] Mohammad Peikari, Sherine Salama, Sharon Nofech-Mozes, and Anne L. Martel. A cluster-then-label semi-supervised learning approach for pathology image classification. *Scientific Reports*, 8, 2018.
- [11] Izzat Alsmadi and Ikdam Alhami. Clustering and classification of email contents. *J. King Saud Univ. Comput. Inf. Sci.*, 27:46–57, 2015.
- [12] Mehryar Mohri, Afshin Rostamizadeh, and Ameet Talwalkar. *Foundations of machine learning*. MIT Press, 2012.
- [13] Sibylle Hess, Wouter Duivestijn, and Decebal Constantin Mocanu. Softmax-based classification is k-means clustering: Formal proof, consequences for adversarial attacks, and improvement through centroid based tailoring. *ArXiv*, abs/2001.01987, 2020.
- [14] Hind Elouedi, Walid Meliani, Zied Elouedi, and Nahla Ben Amor. A hybrid approach based on decision trees and clustering for breast cancer classification. *2014 6th International Conference of Soft Computing and Pattern Recognition (SoCPaR)*, pages 226–231, 2014.
- [15] Martin Vincent and Niels Richard Hansen. Sparse group lasso and high dimensional multinomial classification. *Comput. Stat. Data Anal.*, 71:771–786, 2014.
- [16] Andrea Visentin, Alessia Nardotto, and Barry O’Sullivan. Predicting judicial decisions: A statistically rigorous approach and a new ensemble classifier. *2019 IEEE 31st International Conference on Tools with Artificial Intelligence (ICTAI)*, pages 1820–1824, 2019.
- [17] Ahmed M. Mahfouz, Abdullah Abuhussein, Deepak Venugopal, and Sajjan G. Shiva. Ensemble classifiers for network intrusion detection using a novel network attack dataset. *Future Internet*, 12:180, 2020.
- [18] William H. Beluch, Tim Genewein, A. Nürnberger, and Jan M. Köhler. The power of ensembles for active learning in image classification. *2018 IEEE/CVF Conference on Computer Vision and Pattern Recognition*, pages 9368–9377, 2018.
- [19] Ivan Titov, A. Klementiev, Kevin Small, and Dan Roth. Unsupervised aggregation for classification problems with large numbers of categories. In *AISTATS*, 2010.
- [20] Botao Hao, Will Wei Sun, Yufeng Liu, and Guang Cheng. Simultaneous clustering and estimation of heterogeneous graphical models. *Journal of machine learning research : JMLR*, 18, 2017.
- [21] Guo-Jun Qi, Qi Tian, and Thomas S. Huang. Locality-sensitive support vector machine by exploring local correlation and global regularization. *CVPR 2011*, pages 841–848, 2011.
- [22] Lubor Ladicky and Philip H. S. Torr. Locally linear support vector machines. In *ICML*, 2011.
- [23] Kilian Q. Weinberger and Lawrence K. Saul. Distance metric learning for large margin nearest neighbor classification. In *NIPS*, 2005.
- [24] Kun Song, Feiping Nie, Junwei Han, and Xuelong Li. Parameter free large margin nearest neighbor for distance metric learning. In *AAAI*, 2017.
- [25] Weiling Cai, Songcan Chen, and Daoqiang Zhang. A simultaneous learning framework for clustering and classification. *Pattern Recognit.*, 42:1248–1259, 2009.

- [26] Chaohe Zhang, Xin Gao, Liantao Ma, Yasha Wang, Jiangtao Wang, and Wen Tang. Grasp: Generic framework for health status representation learning based on incorporating knowledge from similar patients. In *AAAI*, 2021.
- [27] Changhee Lee and Mihaela Van Der Schaar. Temporal phenotyping using deep predictive clustering of disease progression. In *ICML*, 2020.
- [28] Stuart P. Lloyd. Least squares quantization in pcm. *IEEE Trans. Inf. Theory*, 28:129–136, 1982.
- [29] Adam Coates and A. Ng. Learning feature representations with k-means. In *Neural Networks: Tricks of the Trade*, 2012.
- [30] Bo Yang, Xiao Fu, N. Sidiropoulos, and Mingyi Hong. Towards k-means-friendly spaces: Simultaneous deep learning and clustering. In *ICML*, 2017.
- [31] Bo Yang, Xiao Fu, and N. Sidiropoulos. Learning from hidden traits: Joint factor analysis and latent clustering. *IEEE Transactions on Signal Processing*, 65:256–269, 2017.
- [32] Jianwei Yang, Devi Parikh, and Dhruv Batra. Joint unsupervised learning of deep representations and image clusters. *2016 IEEE Conference on Computer Vision and Pattern Recognition (CVPR)*, pages 5147–5156, 2016.
- [33] Peter L Bartlett and Shahar Mendelson. Rademacher and gaussian complexities: Risk bounds and structural results. *JMLR*, 2002.
- [34] Matus Telgarsky and Andrea Vattani. Hartigan’s method: k-means clustering without voronoi. In *AISTATS*, 2010.
- [35] Xifeng Guo, Long Gao, Xinwang Liu, and Jianping Yin. Improved deep embedded clustering with local structure preservation. In *IJCAI*, 2017.
- [36] Mathilde Caron, Ishan Misra, Julien Mairal, Priya Goyal, Piotr Bojanowski, and Armand Joulin. Unsupervised learning of visual features by contrasting cluster assignments. *ArXiv*, abs/2006.09882, 2020.
- [37] Feng Wang, Jian Cheng, Weiyang Liu, and Haijun Liu. Additive margin softmax for face verification. *IEEE Signal Processing Letters*, 25(7):926–930, 2018.
- [38] Feng Wang, Xiang Xiang, Jian Cheng, and Alan Loddon Yuille. Normface: L2 hypersphere embedding for face verification. *Proceedings of the 25th ACM international conference on Multimedia*, 2017.
- [39] Matthew A Reyna, Chris Josef, Salman Seyedi, Russell Jeter, Supreeth P Shashikumar, M Brandon Westover, Ashish Sharma, Shamim Nemati, and Gari D Clifford. Early prediction of sepsis from clinical data: the physionet/computing in cardiology challenge. In *CinC*, 2019.
- [40] M. Lee et. al. WiDS (Women in Data Science) Datathon 2020: ICU Mortality Prediction, 2020.
- [41] M. Lichman. Uci repository. *UCI*, 2013.
- [42] Alistair EW Johnson, Tom J Pollard, Lu Shen, Liwei H Lehman, Mengling Feng, Mohammad Ghassemi, Benjamin Moody, Peter Szolovits, Leo Anthony Celi, and Roger G Mark. Mimic-iii, a freely accessible critical care database. *Scientific data*, 3(1):1–9, 2016.
- [43] Ikaro Silva, George B. Moody, Daniel J. Scott, Leo Anthony Celi, and Roger G. Mark. Predicting in-hospital mortality of icu patients: The physionet/computing in cardiology challenge 2012. *2012 Computing in Cardiology*, pages 245–248, 2012.
- [44] Ikaro Silva, George B. Moody, Daniel J. Scott, Leo Anthony Celi, and Roger G. Mark. Predicting in-hospital mortality of icu patients: The physionet/computing in cardiology challenge 2012. *2012 Computing in Cardiology*, pages 245–248, 2012.
- [45] James Morrill, Andrey Kormilitzin, Alejo J. Nevado-Holgado, Sumanth Swaminathan, Sam, Howison, and Terry Lyons. The signature-based model for early detection of sepsis from electronic health records in the intensive care unit. *2019 Computing in Cardiology (CinC)*, pages Page 1–Page 4, 2019.
- [46] Xiangrui Li, Dongxiao Zhu, and Phillip Levy. Predicting clinical outcomes with patient stratification via deep mixture neural networks. *AMIA Summits on Translational Science*, 2020.
- [47] Manchek A Wong and JA Hartigan. Algorithm as 136: A k-means clustering algorithm. *Journal of the Royal Statistical Society. Series C (Applied Statistics)*, 1979.
- [48] Sanjoy Dasgupta. *The hardness of k-means clustering*. University of California, 2008.
- [49] F. Pedregosa, G. Varoquaux, A. Gramfort, V. Michel, B. Thirion, et al. Scikit-learn: Machine learning in Python. *JMLR*, 2011.
- [50] J. Gou, B. Yu, S. J. Maybank, and D. Tao. Knowledge distillation: A survey. *International Journal of Computer Vision*, 129(6):1789–1819, 2021.

Appendix

10 CAC details

10.1 Class Separability

We use a simple heuristic to measure class separability within each cluster. For each cluster C_j ($j \in [k]$), we define: *cluster centroid*: $\mu(C_j) := |C_j|^{-1} \sum_{x \in C_j} x_i$, *positive centroid*: $\mu^+(C_j) := (\sum_{x_i \in C_j} y_i)^{-1} \sum_{x_i \in C_j} y_i x_i$, and *negative centroid*: $\mu^-(C_j) := (\sum_{x_i \in C_j} (1 - y_i))^{-1} \sum_{x_i \in C_j} (1 - y_i) x_i$.

Class separability is defined by considering the distance between positive and negative centroids within each cluster. Figure 7 shows two clusters C_1 and C_2 . C_1 has greater class separation while in C_2 , the data points are more intermingled and thus their centroids are closer. Thus, $\|\mu_1^+ - \mu_1^-\| > \|\mu_2^+ - \mu_2^-\|$.

10.2 Finding the clusters

The most common heuristic to find k -means clusters is Lloyd’s Algorithm [28]. It begins with an initial clustering and iteratively computes cluster centroids and assigns points to clusters corresponding to their closest centroids. However, using this heuristic with our proposed cost may not guarantee convergence. (See our discussion after Theorem 11.5). Instead, we adopt an approach based on Hartigan’s method [47]. For k -means clustering, Hartigan’s method proceeds point by point in a greedy manner. Each point is reassigned to a cluster such that the overall cost is reduced.

In our setting, denote the cost of merging a point x to some cluster C_q as $\Gamma^+(C_q, x) = \phi(C_q \cup \{x\}) - \phi(C_q)$. Symmetrically, denote the cost of removing a point x from some cluster C_p as $\Gamma^-(C_p, x) = \phi(C_p \setminus \{x\}) - \phi(C_p)$.

The cost function of cluster C_j with respect to point i is calculated as $\|x_i - \mu_j\|^2 - \alpha \|\mu^+(C_j) - \mu^-(C_j)\|^2$. α is a hyperparameter which controls the weightage given to the class separation parameter. Typical value of α lies within the range 0 to 2 but it can vary according to the size of the dataset.

Consequently, define the improvement in cost by moving a point $x \in C_p$ from cluster C_p to cluster C_q to be $\Phi(x; C_p, C_q) := \Gamma^+(C_q, x) + \Gamma^-(C_p, x)$. The exact expressions for $\Gamma^+(C_q, x)$ and $\Gamma^-(C_p, x)$ w.r.t x, μ, μ^\pm can be easily derived from above definitions and the CAC cost function (not shown here due to lack of space).

The main idea is from Hartigan’s method of clustering [34]: It begins with an initial clustering (k -means found clusters) and then proceeds iteratively in rounds. In each round, all points are checked to determine if a point has to be re-assigned to another cluster. For a point in the current iteration, x_i , if moving $x_i \in C_p$ would result in C_p/x_i

having points of only one class, then it is not moved. If not, the cluster C_q that results in the maximum decrease in cost $\Phi(x_i; C_p, C_q)$ is found and x_i is moved from its current cluster C_p to C_q .

In each round, all three centroids for each cluster are updated and once the loss function has become stagnant, the algorithm is considered to have converged. Base classifiers are then trained on the clusters found and are used for predicting labels for the unseen test data.

Classifiers f_j are trained to minimize their corresponding supervised training loss $\ell(f, C) = \sum_{j=1}^k \ell(f_j, C_j)$. The best collection of classifiers, chosen based on a user-defined performance metric (e.g., training loss or validation set performance), is the final output, along with the corresponding cluster centroids.

The CAC algorithm runs until convergence and outputs the best collection of classifiers f_{best} that minimizes the empirical loss.

Remark (Hartigan vs. Lloyd). For k -means clustering, both Lloyd’s method and Hartigan’s method converge since the cost function always decreases monotonically with each update. Note that Lloyd’s method does not consider the change in centroids while updating the assignment of a point, and instead, directly assign points to their current closest centroids. In our setting, Lloyd’s method can similarly fix all centroids, compute a new assignment, and update the centroids accordingly. For instance, replacing the assignment rule of x_i in Algorithm 1 by $q := \operatorname{argmin}_j \|x_i - \mu(C_j)\|^2 - \alpha \cdot \|\mu^+(C_j) - \mu^-(C_j)\|^2$. However, our cost function contains an additional squared distance term between positive and negative centroids, i.e., $-\alpha \cdot \|\mu^+(C_j) - \mu^-(C_j)\|^2$. There is no guarantee that this term monotonically decreases by Lloyd’s method during the update of $\mu^+(C_j)$ and $\mu^-(C_j)$ after an assignment. Hence, it is non-trivial to ensure and prove the convergence of Lloyd’s method with our cost function. However, with the use of Hartigan’s method, convergence is ensured by design. As for the rate of convergence, empirical experiments demonstrate that the rate of convergence is positively related to α .

10.3 CAC Prediction

CAC outputs a set of cluster representatives denoted by their centroids and the trained classifiers associated with those clusters. To make predictions for a test point \hat{x} , the first step is to find the cluster to which the test point is most likely to belong. This can be done by assigning the test point to a cluster represented by the ‘closest’ centroid C_j in the data space i.e. $j = \operatorname{argmin}_l \|\hat{x} - \mu_l\|^2$. The corresponding classifier f_j can then be used to predict $\hat{y} = f_j(\hat{x})$.

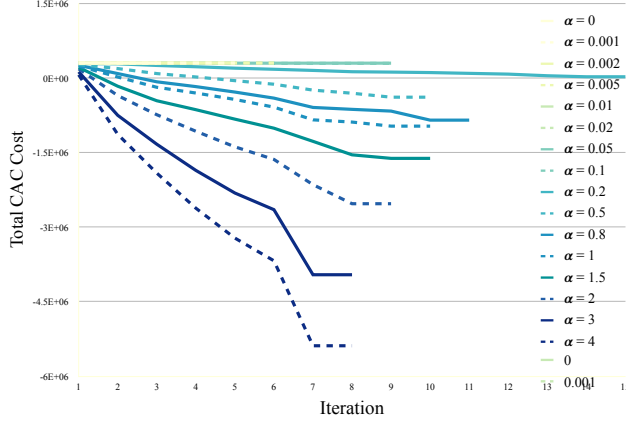
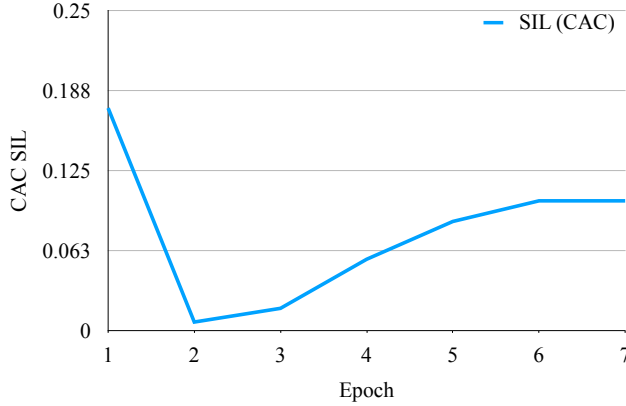

 Figure 4: Total CAC cost v/s # of iterations for different α .


Figure 5: CAC clustering Silhouette score v/s training epochs

11 Proof of Theorems

11.1 Proof of Theorem 1

The following lemma is from [12, 33, Theorem 3.1]:

Lemma 1. Let \mathcal{F} be a set of maps $x \mapsto f(x)$. Suppose that $0 \leq \ell(q, y) \leq \lambda$ for any $q \in \{f(x) : f \in \mathcal{F}, x \in \mathcal{X}\}$ and $y \in \mathcal{Y}$. Then, for any $\delta > 0$, with probability at least $1 - \delta$ (over an i.i.d. draw of m i.i.d. samples $((x_i, y_i))_{i=1}^m$), the following holds: for all maps $f \in \mathcal{F}$,

$$\mathbb{E}_{x,y}[\ell(f(x), y)] \leq \frac{1}{m} \sum_{i=1}^m \ell(f(x_i), y_i) + 2\hat{\mathcal{R}}_m(\ell \circ \mathcal{F}) + 3\lambda \sqrt{\frac{\ln(1/\delta)}{2m}}, \quad (3)$$

where $\hat{\mathcal{R}}_m(\ell \circ \mathcal{F}) := \mathbb{E}_\sigma[\sup_{f \in \mathcal{F}} \frac{1}{m} \sum_{i=1}^m \sigma_i \ell(f(x_i), y_i)]$ and $\sigma_1, \dots, \sigma_m$ are independent uniform random variables taking values in $\{-1, 1\}$.

We can use Lemma 1 to prove the following:

Theorem 1. Let \mathcal{F}_j be a set of maps $x \in C_j \mapsto f_j(x)$. Let $\mathcal{F} = \{x \mapsto f(x) : f(x) = \sum_{j=1}^K \mathbb{1}\{x \in C_j\} f_j(x), f_j \in \mathcal{F}_j\}$. Suppose that $0 \leq \ell(q, y) \leq \lambda_j$ for any $q \in \{f(x) : f \in \mathcal{F}_j, x \in C_j\}$ and $y \in \mathcal{Y}_j$. Then, for any $\delta > 0$, with probability at least $1 - \delta$, the following holds: for all maps $f \in \mathcal{F}$,

$$\mathbb{E}_{x,y}[\ell(f(x), y)] \leq \sum_{j=1}^K \Pr(x \in C_j) \left(\frac{1}{m_j} \sum_{i=1}^{m_j} \ell(f(x_i^j), y_i^j) + 2\hat{\mathcal{R}}_{m_j}(\ell \circ \mathcal{F}_j) + 3\lambda_j \sqrt{\frac{\ln(K/\delta)}{2m_j}} \right), \quad (4)$$

where

$\hat{\mathcal{R}}_m(\ell \circ \mathcal{F}_j) := \mathbb{E}_\sigma[\sup_{f_j \in \mathcal{F}_j} \frac{1}{m} \sum_{i=1}^m \sigma_i \ell(f_j(x_i), y_i)]$, $\Pr(x \in C_j) = 1$ if $x \in C_j$ and $\sigma_1, \dots, \sigma_m$ are independent uniform random variables taking values in $\{-1, 1\}$.

Proof of Theorem 1. We have the following.

$$\begin{aligned} \mathbb{E}_{x,y}[\ell(f(x), y)] &= \sum_{j=1}^K \Pr(x \in C_j) \mathbb{E}_{x,y}[\ell(f(x), y) \mid x \in C_j] \\ &= \sum_{j=1}^K \Pr(x \in C_j) \mathbb{E}_{x,y}[\ell(f_j(x), y) \mid x \in C_j]. \end{aligned} \quad (5)$$

Since the conditional probability distribution is a probability distribution, we apply Lemma 1 to each term and take a union bound to obtain the following: for any $\delta > 0$, with probability at least $1 - \delta$, for all $j \in \{1, \dots, K\}$ and all $f_j \in \mathcal{F}_j$,

$$\begin{aligned} \mathbb{E}_{x,y}[\ell(f_j(x), y) \mid x \in C_j] &\leq \frac{1}{m_j} \sum_{i=1}^{m_j} \ell(f_j(x_i^j), y_i^j) + 2\hat{\mathcal{R}}_{m_j}(\ell \circ \mathcal{F}_j) + 3\lambda_j \sqrt{\frac{\ln(K/\delta)}{2m}} \\ &= \frac{1}{m_j} \sum_{i=1}^{m_j} \ell(f(x_i^j), y_i^j) + 2\hat{\mathcal{R}}_{m_j}(\ell \circ \mathcal{F}_j) + 3\lambda_j \sqrt{\frac{\ln(K/\delta)}{2m}}. \end{aligned}$$

Thus, using (5), we sum up both sides with factors $\Pr(x \in C_j)$ to yield:

$$\begin{aligned} \mathbb{E}_{x,y}[\ell(f(x), y)] &= \sum_{j=1}^K \Pr(x \in C_j) \mathbb{E}_{x,y}[\ell(f_j(x), y) \mid x \in C_j] \\ &\leq \sum_{j=1}^K \Pr(x \in C_j) \left(\frac{1}{m_j} \sum_{i=1}^{m_j} \ell(f(x_i^j), y_i^j) + 2\hat{\mathcal{R}}_{m_j}(\ell \circ \mathcal{F}_j) + 3\lambda_j \sqrt{\frac{\ln(K/\delta)}{2m}} \right) \end{aligned} \quad (6)$$

□

11.2 Proof of Lemma 2

Lemma 2. For d dimensional vectors \mathbf{u}, \mathbf{v} and β , $\frac{\partial \Delta}{\partial \|\mathbf{u}\|} < 0$ for $\Delta = A - (B\beta\mathbf{u} + C\beta\mathbf{v})$ if $\beta_i u_i > 0, \forall i \in \{1, 2, \dots, d\}$ and $A, B > 0$.

Proof. Let u_i be the i^{th} element of \mathbf{u} . Expanding $\frac{\partial \Delta}{\partial \|\mathbf{u}\|}$ using chain rule, we get

$$\frac{\partial \Delta}{\partial \|\mathbf{u}\|} = \frac{\partial \Delta}{\partial \mathbf{u}} \cdot \frac{\partial \mathbf{u}}{\partial \|\mathbf{u}\|} = -B\beta \cdot \frac{\partial \mathbf{u}}{\partial \|\mathbf{u}\|} \quad (\text{Since } \frac{\partial \Delta}{\partial \mathbf{u}} = -B\beta\mathbf{u})$$

Let u_i denote the i^{th} element of \mathbf{u} . Then, from the definition of vector derivatives we have,

$$\begin{aligned} \frac{\partial \mathbf{u}}{\partial \|\mathbf{u}\|} &= \begin{bmatrix} \frac{\partial u_1}{\partial \|\mathbf{u}\|} & \frac{\partial u_2}{\partial \|\mathbf{u}\|} & \dots & \frac{\partial u_d}{\partial \|\mathbf{u}\|} \end{bmatrix} \\ &= \begin{bmatrix} \left(\frac{\partial \|\mathbf{u}\|}{\partial u_1}\right)^{-1} & \left(\frac{\partial \|\mathbf{u}\|}{\partial u_2}\right)^{-1} & \dots & \left(\frac{\partial \|\mathbf{u}\|}{\partial u_d}\right)^{-1} \end{bmatrix} \\ &= \|\mathbf{u}\| \begin{bmatrix} \frac{1}{u_1} & \frac{1}{u_2} & \dots & \frac{1}{u_d} \end{bmatrix} \end{aligned}$$

Thus, $\frac{\partial \Delta}{\partial \|\mathbf{u}\|} = -B \cdot \|\mathbf{u}\| \cdot \sum_{i=1}^d \frac{\beta_i}{u_i}$, where $u_i = \mu_i^+ - \mu_i^-$ and

$$v_i = \mu_i^+ + \mu_i^-.$$

Since $\beta \cdot \mu^+ > 0$ and $\beta \cdot \mu^- < 0$, it implies that $\beta \cdot \mathbf{u} > 0$. Assuming that every dimension of \mathbf{u} lies on the same side of regression plane β as the original point, i.e. $\beta_i u_i = \beta_i > 0, \forall i, \frac{\beta_i}{u_i} > 0 \forall i$, then $\frac{\partial \Delta}{\partial \|\mathbf{u}\|} < 0$ as B and $\|\mathbf{u}\|$. Thus under above assumption, we prove that Δ decreases as $\|\mathbf{u}\|$ increases. \square

11.3 Proof of Theorem 2

Theorem 2. Let $X = (x_1, x_2, \dots, x_N)$ be a training dataset with n records $x_i \in \mathbb{R}^d$ together with binary labels $y_i \in \{0, 1\}$. Define the log-loss over the entire dataset as :

$$\ell(X) = -\sum_i y_i \ln(p(x_i)) + (1 - y_i) \ln(1 - p(x_i))$$

where $p(x_i) = [1 + \exp(-\beta x_i)]^{-1}$ and $\beta = \operatorname{argmin}_{\beta} \ell(X)$. Then,

$$C_1 - (C_3 \beta \mu^+ - C_4 \beta \mu^-) \leq \ell(X) \leq C_2 - (C_3 \beta \mu^+ - C_4 \beta \mu^-)$$

where $C_1 = N \ln(2)$, $C_2 = N \ln(1 + \exp(c)) - \frac{Nc}{2}$, $C_3 = \frac{N^+}{2}$, $C_4 = \frac{N^-}{2}$, $N^+ = \sum_{x_i \in X} y_i$, $N^- = \sum_{x_i \in X} (1 - y_i)$ and $c = \operatorname{argmax}_i \|\beta x_i\|$.

Proof. Lower Bound Let $\ell(X, y) = \sum_{y_i=1} \ell^+(x_i) + \sum_{y_i=0} \ell^-(x_i)$ s.t.

$$\ell^+(x_i) = -\ln(p_i), \ell^-(x_i) = -\ln(1 - p_i) \quad (7)$$

Applying Jensen's inequality on ℓ^+ and ℓ^- ,

$$\begin{aligned} \ell(X) &= \sum_{x_i \in X^+} \ell^+(x_i) + \sum_{x_i \in X^-} \ell^-(x_i) \\ &= -\sum_{y_i=1} \ln[1 + \exp(-\beta x_i)]^{-1} - \sum_{y_i=0} \ln[1 - (1 + \exp(-\beta x_i))^{-1}] \quad (\text{By eq. 7}) \end{aligned}$$

$$\begin{aligned} &\geq -N^+ \ln \left[1 + \exp \left(-\beta \cdot \left(\frac{\sum_{x_i \in X^+} x_i}{N^+} \right) \right) \right]^{-1} \\ &\quad - N^- \ln \left[1 - \left(1 + \exp \left(-\beta \cdot \left(\frac{\sum_{x_i \in X^-} x_i}{N^-} \right) \right) \right)^{-1} \right] \\ &\quad (\text{Jensen's inequality for convex functions}) \\ &\geq N^+ \ln[1 + \exp(-\beta \mu^+)] - N^- \ln \left[\frac{\exp(-\beta \mu^-)}{1 + \exp(-\beta \mu^-)} \right] \\ &\quad (\text{Substituting } \mu^+ \text{ and } \mu^-) \\ &\geq N^+ \ln[1 + \exp(-\beta \mu^+)] + N^- \ln[1 + \exp(\beta \mu^-)] \end{aligned}$$

We observe that $\ln(1 + \exp(x)) \geq \ln(2) + \frac{x}{2} \forall x \in \mathbb{R}$ by considering the Taylor series expansion of $\ln(1 + \exp(x))$ at $x = 0$. $\ln(1 + \exp(x)) = \ln(2) + \frac{x}{2} + \frac{x^2}{8} + \mathcal{O}(x^4)$. Then,

$$\begin{aligned} \ell(X) &\geq N^+ \left(\ln(2) - \frac{\beta \mu^+}{2} \right) + N^- \left(\ln(2) + \frac{\beta \mu^-}{2} \right) \\ &\geq N \ln(2) - \frac{1}{2} \cdot (N^+ \beta \mu^+ - N^- \beta \mu^-) \end{aligned}$$

where $C_1 = N \ln(2)$, $C_3 = \frac{N^+}{2}$, $C_4 = \frac{N^-}{2}$.

Upper Bound

Since all points x_i are constrained within their respective clusters, we note that the maximum log-loss for a point x_i labelled as y_i is not unbounded. Let $c = \operatorname{argmax}_i \|\beta x_i\|$. Since ℓ^+ is a monotonically decreasing function and ℓ^- is monotonically increasing, we can bound them using linear functions s^+ and s^- respectively. $s^+ \geq \ell^+$ and $s^- \geq \ell^-$ for all points X^+ and X^- respectively. $s^+(x_i)$ passes through $(-c, \ln(p(-c)))$ and $(c, \ln(p(c)))$. Hence $s^+(x) = K_1 - K_2 \cdot \beta x$ where $K_1, K_2 > 0$. Similarly, $s^-(x) = K_3 + K_4 \cdot \beta x$ where $K_3, K_4 > 0$.

Solving for $K_1 \dots K_4$, we get

$$K_1 = K_3 = \ln(1 + \exp(c)) - \frac{c}{2}, K_2 = K_4 = \frac{1}{2}$$

Then,

$$\begin{aligned}
 \ell(X) &= \sum_{x_i \in X^+} \ell^+(x_i) + \sum_{x_i \in X^-} \ell^-(x_i) \\
 &< \sum_{x_i \in X^+} s^+(x_i) + \sum_{x_i \in X^-} s^-(x_i) \\
 &\leq N^+ s^+ \left(\frac{\sum_{x_i \in X^+} x_i}{N^+} \right) + N^- s^- \left(\frac{\sum_{x_i \in X^-} x_i}{N^-} \right) \\
 &\text{(Jensen's inequality for a linear function)} \\
 &\leq N^+ s^+(\mu^+) + N^- s^-(\mu^-) \\
 &\leq N^+(K_1 - K_2 \cdot \beta \mu^+) + N^-(K_3 + K_4 \cdot \beta \mu^-) \\
 &\leq C_2 - (C_3 \beta \mu^+ - C_4 \beta \mu^-) \text{ (Rearranging terms)}
 \end{aligned}$$

where $C_2 = N \ln(1 + \exp(c)) - \frac{Nc}{2}$ and $C_3 = \frac{N^+}{2}$, $C_4 = \frac{N^-}{2}$. \square

11.4 Proof of Theorem 3

Theorem 3. Let $X = (x_1, x_2, \dots, x_N)$ be a training dataset with n records $x_i \in \mathbb{R}^d$ together with binary labels $y_i \in \{0, 1\}$. Define the AM Softmax loss over the entire dataset as :

$$-\sum_i \log \frac{e^{s \cdot (W_{y_i}^T z_i - m)}}{e^{s \cdot (W_{y_i}^T z_i - m)} + \sum_{j=1, j \neq y_i}^c e^{s W_j^T z_i}}$$

Then,

$$K_1 - \Gamma(K_3 \mu^+ - K_4 \mu^-) \leq \ell(X) \leq K_2 - \Gamma(K_3 \mu^+ - K_4 \mu^-)$$

where $K_1 = N \left(\log 2 + \frac{sm}{2} \right)$, $K_2 = N(1 + sm)$, $K_3 = sN^+$, $K_4 = sN^-$, $N^+ = \sum_{x_i \in X} y_i$, $N^- = \sum_{x_i \in X} (1 - y_i)$ and $\Gamma = W_+^T - W_-^T$.

Proof. Rewriting L_{AM} by collecting all the terms for the positive and negative classes, we get

$$\begin{aligned}
 L_{AM} &= - \sum_{i:y_i=0} \log \frac{e^{s \cdot (W_-^T z_i - m)}}{e^{s \cdot (W_-^T z_i - m)} + e^{s W_+^T x_i}} + \\
 &\quad - \sum_{i:y_i=1} \log \frac{e^{s \cdot (W_+^T z_i - m)}}{e^{s \cdot (W_+^T z_i - m)} + e^{s W_-^T x_i}} \\
 &= \sum_{i:y_i=0} \log 1 + e^{sm + s z_i (W_+ - W_-)} + \\
 &\quad \sum_{i:y_i=1} \log 1 + e^{sm + s z_i (W_- - W_+)}
 \end{aligned}$$

Lower Bound Let $g^+ = \log[1 + e^{sm + s z_i (W_- - W_+)}]$ and $g^- = \log[1 + e^{sm + s z_i (W_+ - W_-)}]$. Note that g^+ and g^- are convex functions. Applying Jensen's inequality on g^+ and g^- we get:

$$\begin{aligned}
 L_{AM} &= \sum_{i:y_i=0} \log[1 + e^{sm + s z_i (W_+ - W_-)}] + \\
 &\quad \sum_{i:y_i=1} \log[1 + e^{sm + s z_i (W_- - W_+)}] \\
 &> N^+ \log[1 + e^{sm + s z \mu^+ (W_+ - W_-)}] + \\
 &\quad N^- \log[1 + e^{sm + s z \mu^- (W_- - W_+)}]
 \end{aligned}$$

Since $\log(1 + e^x) > \log 2 + \frac{x}{2} \forall x$, we can further simplify the above expression.

$$\begin{aligned}
 L_{AM} &> N^- \log[1 + e^{sm + s z \mu^+ (W_+ - W_-)}] + \\
 &\quad N^+ \log[1 + e^{sm + s z \mu^- (W_- - W_+)}] \\
 &> N^- [\log 2 + \frac{1}{2}(sm + s \mu^- (W_+ - W_-))] + \\
 &\quad N^+ [\log 2 + \frac{1}{2}(sm + s \mu^+ (W_- - W_+))] \\
 &> N \left(\log 2 + \frac{sm}{2} \right) - s(W_+ - W_-)[N^+ \mu^+ - N^- \mu^-]
 \end{aligned}$$

Upper Bound For all $x > 0$, $\log(1 + e^x) < 1 + x$. Since $sm + s z_i (W_+ - W_-) > 0$ for all z_i s.t. $y_i = 0$ and $sm + s z_i (W_- - W_+) > 0$ for all z_i s.t. $y_i = 1$ (see [37]), we can safely apply the above mentioned inequality to get an upper bound for L_{AM} .

$$\begin{aligned}
 L_{AM} &= \sum_{i:y_i=0} \log[1 + e^{sm + s z_i (W_+ - W_-)}] + \\
 &\quad \sum_{i:y_i=1} \log[1 + e^{sm + s z_i (W_- - W_+)}] \\
 L_{AM} &< N^+ [1 + sm + s z_i (W_- - W_+)] + \\
 &\quad N^- [1 + sm + s z_i (W_+ - W_-)] \\
 &< (N^+ + N^-)(1 + sm) + s N^- \mu^- (W_+ - W_-) + \\
 &\quad s N^+ \mu^+ (W_- - W_+) \\
 &< N(1 + sm) - s(W_+ - W_-)(N^+ \mu^+ - N^- \mu^-)
 \end{aligned}$$

\square

11.5 Theorem on Convergence of CAC

Theorem 2. Algorithm 1 converges to a local minimum.

Proof. To prove convergence, it suffices to verify that the cost function, that re-assigns point x from cluster C_p to cluster C_q , monotonically decreases at each iteration. This is equivalent to showing $\phi(C_p \setminus \{x_i\}) + \phi(C_q \cup \{x_i\}) < \phi(C_p) + \phi(C_q) \implies (\phi(C_p \setminus \{x_i\}) - \phi(C_p)) + (\phi(C_q \cup \{x_i\}) - \phi(C_q)) < 0$

$$\{\phi(x_i) - \phi(C_q)\} < 0 \implies \Gamma^+(C_q, x) + \Gamma^-(C_p, x) < 0 \implies \Phi(x_i, C_p, C_q) < 0.$$

$\Phi(x_i, C_p, C_q) < 0$ is exactly the update condition for the algorithm that ensures that the total cost function is always decreasing with every point update and in every iteration. If we move $\epsilon < 1$ away from our binary cluster indicator then we do not get a binary result anymore, which is not in the feasible set and which is hence not minimizing the objective. Hence the clustering derived is trivially a local minimum. \square

11.6 Theorem on Time Complexity of CAC

Theorem 3. *The time complexity for each round of CAC is $O(ndk)$.*

Proof. For the time complexity of each round, it suffices to prove the running time for each point x_i is $O(dk)$. For each $j \in [k]$, we denote the centroid, positive centroid and negative centroid of $C_j \cup \{x_i\}$ as $\tilde{\mu}(C_j)$, $\tilde{\mu}^+(C_j)$ and $\tilde{\mu}^-(C_j)$ respectively. Given a cluster C_j and a point $z \in \mathbb{R}^d$, we denote the clustering cost of C w.r.t. z to be

$$g(C_j, z) := \sum_{x \in C_j} \|x - z\|^2.$$

A standard result from the k -means literature [48] is the following bias-variance decomposition of the k -means cost function:

$$g(C_j, z) = \phi(C_j, \mu(C_j)) + |C_j| \cdot \|\mu(C_j) - z\|^2.$$

Note that the above result holds for CAC cluster cost function also as can be shown easily by a little algebra. Based on this property, we have

$$\begin{aligned} & \Gamma^+(C_j, x_i) \\ &= \|\tilde{\mu} - x_i\|^2 + |C_j| \cdot \|\tilde{\mu}(C_j) - \mu(C_j)\|^2 \\ & \quad + \alpha |C_j| \cdot \|\mu^+(C_j) - \mu^-(C_j)\|^2 \\ & \quad - \alpha (|C_j| + 1) \cdot \|\tilde{\mu}^+(C_j) - \tilde{\mu}^-(C_j)\|^2 \\ & \Gamma^-(C_j, x_i) \\ &= -\|\mu(C_j) - x_i\|^2 - (|C_j| - 1) \|\tilde{\mu}(C_j) - \mu(C_j)\|^2 \\ & \quad + \alpha |C_j| \cdot \|\mu^+(C_j) - \mu^-(C_j)\|^2 \\ & \quad - \alpha (|C_j| - 1) \cdot \|\tilde{\mu}^+(C_j) - \tilde{\mu}^-(C_j)\|^2 \end{aligned}$$

Then it suffices to prove that both $\Gamma^+(C_j, x_i)$ and $\Gamma^-(C_j, x_i)$ can be computed in $O(d)$ time, which implies $O(dk)$ time for computing $q := \operatorname{argmin}_j \Phi(x_i; C_p, C_j)$. Moreover, by the above formulations, it suffices to prove that $\tilde{\mu}(C_j)$, $\tilde{\mu}^+(C_j)$ and $\tilde{\mu}^-(C_j)$ can be computed in $O(d)$ time. Note that $\tilde{\mu}(C_p) = \frac{|C_p| \cdot \mu(C_p) - x_i}{|C_p| - 1}$ and $\tilde{\mu}(C_j) =$

$\frac{|C_j| \cdot \mu(C_j) + x_i}{|C_j| + 1}$ for $j \neq p$. Hence, each $\tilde{\mu}(C_j)$ can be computed in $O(d)$ time. We discuss the following two cases for the computation of $\tilde{\mu}^+(C_j)$ and $\tilde{\mu}^-(C_j)$.

- Case $y_i = 1$. We have that $\tilde{\mu}^+(C_p) = \frac{(\sum_{x_l \in C_p} y_l) \cdot \mu_p^+ - x_i}{\sum_{x_l \in C_p} y_l - 1}$ and $\tilde{\mu}^-(C_p) = \mu^-(C_p)$. For $j \neq p$, we have that $\tilde{\mu}^+(C_j) \leftarrow \frac{(\sum_{x_l \in C_j} y_l) \cdot \mu_j^+ + x_i}{\sum_{x_l \in C_j} y_l + 1}$ and $\tilde{\mu}^-(C_j) = \mu^-(C_j)$.
- Case $y_i = 0$. We have that $\tilde{\mu}^-(C_p) \leftarrow \frac{(\sum_{x_l \in C_p} (1 - y_l)) \cdot \mu_p^- - x_i}{\sum_{x_l \in C_p} (1 - y_l) - 1}$ and $\tilde{\mu}^+(C_p) = \mu^+(C_p)$. For $j \neq p$, we have that $\tilde{\mu}^-(C_j) \leftarrow \frac{(\sum_{x_l \in C_j} (1 - y_l)) \cdot \mu_j^- + x_i}{\sum_{x_l \in C_j} (1 - y_l) + 1}$ and $\tilde{\mu}^+(C_j) = \mu^+(C_j)$.

By the above update rules, both $\tilde{\mu}^+(C_j)$ and $\tilde{\mu}^-(C_j)$ can be computed in $O(d)$ time, which completes the proof. \square

11.7 Hyperparameter Details

CAC's α values are found by performing a 5-fold CV Grid search (see App. 11.7). Table 4 shows the tuned values of α used by different variants of CAC on different datasets. We find these values by performing a 5-fold Grid search cross validation. Figure 4 shows how the CAC cost function decreases monotonically (as proved in Theorem 11.5) over iterations for different values of α .

11.8 Results on Synthetic Data

We analyse how the performance of CAC depends on the following data/algorithm parameters:

1. Inner Class Separation (*ICS*): Distance between class centroids in an individual cluster.
2. Outer Cluster Separation (*OCS*): Distance between cluster centroids.
3. Number of natural clusters in the dataset (K).
4. Number of classifiers used in CAC (k), i.e., the number of clusters used as input.

To study the performance of CAC as a function of these 4 parameters, we modify the `make_classification` function of *sklearn* library [49], to generate custom datasets with varying ICS, OCS, and K . We choose Logistic Regression (LR) as the base classifier for CAC while testing its performance on the synthetic dataset. The range of these parameters in our simulations is as follows: $ICS \in \{0, 0.2, 0.5, 1, 1.5, 2\}$, $OCS \in \{1, 1.5, 2\}$, $K \in \{2, 3, 5, 10, 15, 20, 30\}$ and $k \in \{2, 3, 4, 5\}$. We run CAC+LR for all combinations of parameters.

Figure 6 presents the results of the experiments. In each subfigure, the results are averaged over all the parameters

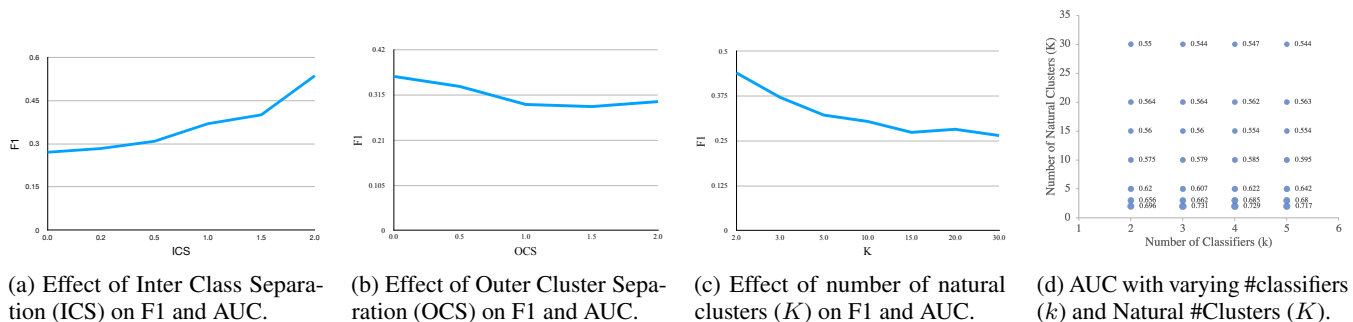


Figure 6: Evaluating the effect of different parameters on the performance of CAC

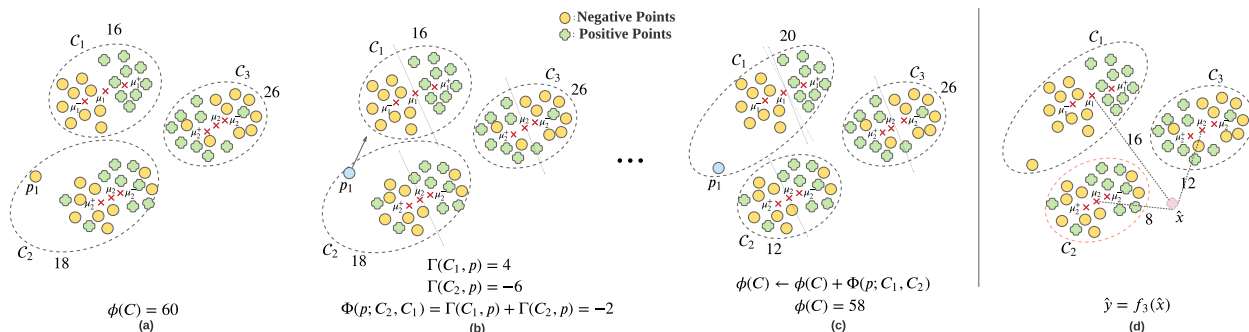


Figure 7: CAC problem setting (with dummy values for illustrative purposes): (a) The total CAC cost of this clustering is 60; (b) Point p_1 is selected to be reassigned to cluster C_1 based on the cluster update equations; (c) p_1 is assigned to C_1 and the cost functions of C_1 and C_2 are updated; (d) At testing time, \hat{x} is assigned to cluster C_2 as it lies nearest to \hat{x} .

 Table 4: Tuned α values used for CAC in experiments found after 5-fold GridCV search

Classifier	LR	SVM	LDA	Perceptron	RF	KNN	SGD	Ridge	XGB
Diabetes	2.5	2.5	2.5	2.5	2.5	2.5	2.5	2.5	3
CIC	0.05	0.5	0.05	0.5	0.5	0.5	0.01	0.5	0.01
WID-M	0.05	0.5	0.05	0.5	0.5	0.5	0.01	0.5	0.01

not shown in the axes. In Figure 6a, note that the performance of CAC improves as Inner Class Separation within the clusters increases. This is in line with our hypothesis that if the classes are well separated within the clusters, then it will improve the performance of the classifiers. The performance of CAC does not depend much on the Outer Cluster Separation (Figure 6b). This is also expected as a classifier will be relatively unaffected by the presence of another cluster, irrespective of its distance as the data in that cluster is not a part of its training set.

As the number of natural clusters in the dataset increases, the performance of CAC decreases (Figure 6c). This phenomenon is expected from linear classifiers as they cannot handle nonlinearities in data. Hence, dividing the data into multiple groups will decrease the piece-wise nonlinearity and the overall algorithm will work better [2]. In Figure 6d, we observe that the results are better for the cases when

$k \geq K$ (i.e., closer to the points near the x-axis). This shows that the performance is better when the number of clusters given as input is not less than the natural clusters in the data, compared to the case when the input number of clusters is less than the natural number of clusters. In the latter case, each (linear) classifier has to learn a non-linear boundary due to the intrinsic cluster structure that leads to a decrease in the performance.

11.9 Results of CAC evaluated on Real Datasets

We use 9 different base classifiers, implemented by *sklearn* library (BSD licenced): LR, Linear SVM, XGBoost (#estimators = 10), Linear Discriminant Analysis (LDA), single Perceptron, Random Forest (#trees = 10), k Nearest Neighbors ($k = 5$), SGD classifier and Ridge classifier (Ridge regressor predicting over the range $[-1, 1]$) as a baseline directly and with k -means (KM+X) in a ‘cluster-then-predict’

Table 5: F1 scores of CAC compared against baseline and k -means+X for different base classifiers on different datasets evaluated on a separate held out testing dataset. Highlighted values signify the best result in that category.

Dataset/Classifier	Diabetes	CIC	WID-M
LR	0.111	0.443	0.398
KM + LR	0.503	0.492	0.41
CAC + LR	0.505	0.492	0.41
SVM	0.523	0.255	0.152
KM + SVM	0.116	0.426	0.354
CAC + SVM	0.506	0.452	0.332
XGB (n_est=10)	0.236	0.454	0.41
KM + XGB	0.358	0.486	0.453
CAC + XGB	0.506	0.49	0.457
LDA	0.112	0.479	0.46
KM + LDA	0.24	0.497	0.427
CAC + LDA	0.506	0.492	0.419
Perceptron	0.349	0.421	0.346
KM + Perceptron	0.333	0.375	0.342
CAC + Perceptron	0.506	0.45	0.331
RF (n_tree=10)	0.406	0.308	0.345
KM + RF	0.407	0.313	0.347
CAC + RF	0.505	0.449	0.332
KNN	0.406	0.218	0.219
KM + KNN	0.407	0.235	0.237
CAC + KNN	0.506	0.45	0.331
SGD	0.204	0.433	0.387
KM + SGD	0.198	0.444	0.383
CAC + SGD	0.506	0.432	0.393
Ridge	0.104	0.347	0.285
KM + Ridge	0.116	0.372	0.294
CAC + Ridge	0.506	0.45	0.331

approach. We evaluate CAC on the Diabetes, WID-M and CIC datasets due to computational considerations related to large sizes of the ARDS and Sepsis datasets.

12 DEEPCAC Training Details

Updating Clustering Parameters For optimizing the clustering loss, we follow the procedure defined in [30]. For fixed network parameters and cluster assignment matrix M , the assignment vectors of the current sample, i.e., s_i , are updated in an online fashion. Specifically, s_i is updated as follows:

$$s_{i,j} = \begin{cases} 1, & \text{if } j = \operatorname{argmin}_l \|f(x_i) - \mu_l\|^2 \\ 0, & \text{otherwise} \end{cases}$$

In [30], the authors update the cluster centroids in an online

manner instead of simply taking the average of every mini-batch as the current minibatch might not be representative of the global cluster structure. So the cluster centroids are updated as follows by a simple gradient step:

$$\mu_j \leftarrow \mu_j - \frac{1}{c_k^i} (\mu_j - f(x_i)) s_{k,i}$$

where c_k^i is the count of the number of times algorithm assigned a sample to cluster k before handling the incoming sample x_i . The class cluster centroids μ_k^b are also updated in a similar, online manner due to the above mentioned reasons.

Updating Autoencoder’s weights. For fixed (M, s_i) , the subproblem of optimizing $(\mathcal{W}, \mathcal{U})$ is similar to training an SAE – but with an additional loss term on clustering performance. Modern deep learning libraries like PyTorch allow us to easily backpropagate both the losses simultaneously. To implement SGD for updating the network parameters, we look at the problem w.r.t. the incoming data x_i :

$$\min_{\mathcal{U}, \mathcal{W}} L^i = \ell(g(f(x_i)), x_i) + \beta \|f(x_i) - Ms_i\| + \alpha \sum_{j=1}^k L_{AM}$$

The gradient of the above function over the network parameters is easily computable, i.e., $\nabla X_{\mathcal{J}} L_i = \frac{\partial \ell(g(f(x_i); \mathcal{W}); \mathcal{U})}{\partial \mathcal{J}} + \alpha \frac{\partial f(x_i)}{\partial \mathcal{J}} (f(x_i) - Ms_i)$, where $\mathcal{J} = (\mathcal{W}, \mathcal{U}, \mathcal{V})$ is a collection of network parameters and the gradients $\frac{\partial l}{\partial \mathcal{J}}$ can be calculated by back-propagation. Then, the network parameters are updated by

$$\mathcal{J} \leftarrow \mathcal{J} - \tau \nabla_{\mathcal{J}} L^i$$

where τ is the diminishing learning rate.

13 Extended Results

Table 6 present the AUC score (5-fold averaged on test dataset) of DEEPCAC and baselines. DEEPCAC beats GRASP in 5 out of 6 experiments.

14 Case Study: ICU Length of Stay Prediction

As a case study, we illustrate the use of DEEPCAC in the CIC-LOS ICU Length of Stay (LoS) prediction data for $k = 3$ clusters. Since we are clustering with a view to induce class separability by making use of training labels, the clusters are influenced by the target label, i.e., LoS indicator, and thus by design DEEPCAC is expected to find LoS subtypes. In other words, we expect the inferred clusters to have

Table 6: AUC of DEEPCAC and other baselines. Best values in **bold**. KM, DCN, and IDEC use the same local classifier as used by DEEPCAC.

Dataset	k	KM-Z –	DCN-Z (2017)	IDEC-Z (2017)	DMNN (2020)	AC-TPC (2020)	GRASP (2021)	DEEPCAC (Ours)
Diabetes	2	0.534 ± 0.012	0.571 ± 0.004	0.565 ± 0.007	0.536 ± 0.005	0.0 ± 0.0	0.569 ± 0.006	0.57 ± 0.006
	3	0.517 ± 0.02	0.569 ± 0.003	0.558 ± 0.012	0.546 ± 0.007	0.540 ± 0.0	0.565 ± 0.005	0.573 ± 0.004
	4	0.508 ± 0.027	0.569 ± 0.003	0.564 ± 0.007	0.545 ± 0.008	0.5 ± 0.0	0.561 ± 0.004	0.568 ± 0.005
CIC	2	0.606 ± 0.036	0.7 ± 0.054	0.766 ± 0.053	0.737 ± 0.039	0.0 ± 0.0	0.827 ± 0.015	0.82 ± 0.021
	3	0.535 ± 0.059	0.705 ± 0.033	0.657 ± 0.039	0.762 ± 0.026	0.757 ± 0.0	0.81 ± 0.022	0.815 ± 0.027
	4	0.549 ± 0.052	0.681 ± 0.043	0.687 ± 0.029	0.731 ± 0.039	0.782 ± 0.0	0.799 ± 0.023	0.811 ± 0.013
CIC-LoS	2	0.576 ± 0.007	0.625 ± 0.017	0.638 ± 0.012	0.61 ± 0.007	0.0 ± 0.0	0.654 ± 0.02	0.664 ± 0.005
	3	0.524 ± 0.026	0.611 ± 0.022	0.596 ± 0.028	0.617 ± 0.012	0.630 ± 0.0	0.65 ± 0.026	0.663 ± 0.01
	4	0.512 ± 0.02	0.625 ± 0.025	0.623 ± 0.012	0.615 ± 0.009	0.601 ± 0.0	0.639 ± 0.025	0.663 ± 0.005
ARDS	2	0.605 ± 0.044	0.658 ± 0.052	0.705 ± 0.01	0.584 ± 0.041	–	0.457 ± 0.03	0.716 ± 0.022
	3	0.546 ± 0.044	0.704 ± 0.022	0.648 ± 0.077	0.571 ± 0.036	0.655 ± 0.019	0.443 ± 0.029	0.705 ± 0.019
	4	0.483 ± 0.055	0.593 ± 0.095	0.697 ± 0.019	0.629 ± 0.024	0.647 ± 0.022	0.564 ± 0.119	0.704 ± 0.039
Sepsis	2	0.621 ± 0.033	0.795 ± 0.011	0.792 ± 0.013	0.656 ± 0.021	–	0.495 ± 0.029	0.803 ± 0.014
	3	0.55 ± 0.09	0.782 ± 0.014	0.781 ± 0.007	0.603 ± 0.055	0.714 ± 0.034	0.474 ± 0.008	0.793 ± 0.034
	4	0.549 ± 0.054	0.691 ± 0.077	0.773 ± 0.014	0.631 ± 0.066	0.684 ± 0.05	0.488 ± 0.01	0.794 ± 0.022
WID-M	2	0.783 ± 0.035	0.843 ± 0.044	0.835 ± 0.052	0.722 ± 0.023	0.0 ± 0.0	0.788 ± 0.022	0.854 ± 0.01
	3	0.669 ± 0.068	0.814 ± 0.055	0.799 ± 0.08	0.708 ± 0.022	0.722 ± 0.0	0.762 ± 0.024	0.851 ± 0.006
	4	0.584 ± 0.105	0.795 ± 0.059	0.811 ± 0.053	0.716 ± 0.019	0.734 ± 0.0	0.79 ± 0.015	0.847 ± 0.01

Table 7: Most distinguishing features amongst clusters

Feature	C1 Mean	C2 mean	C3 mean
UrineOutputSum	10.18	11.221	14.81
MechVentLast8Hour	0.424	0.524	0.903
MechVentDuration	1568.97	1762.353	2314.388
WBC_last	10.355	12.284	13.734
GCS_median	14.368	12.732	9.162
Age	62.202	67.46	62.134
Creatinine_last	0.947	1.32	1.657
BUN_last	17.159	25.647	30.013
Albumin_last	3.091	2.984	2.756
WBC_first	10.65	12.509	15.313

different risk factors tailored to each underlying subpopulation. To evaluate this, we examine feature importances for each cluster’s local risk model. We distill the knowledge of local networks into a simpler student model [50], a Gradient Boosting Classifier in our case, which provides importance values of characteristics. Note that the number of clusters need not be the same as number of classes in the target variable as is imposed by the cluster assumption. In Table 8, we list the cluster sizes C_i , the proportion of patients in the three quartiles of Length of Stay (7, 13, 295 hours) and the top 10 most important features in each cluster. We see that, as expected, the risk models created by DEEPCAC deem different sets of features as important for predicting mortality. Out of the 10 most important features, there is 1 feature (PaO2_last) that is common across all 3 clusters and 2 features are common across the two models. Otherwise, each model has 8, 7, and 8 features unique to the respective clusters.

For the above case study, DEEPCAC attains an AUPRC

Table 8: Important Features for mortality prediction in respective clusters. Features common in all three clusters are highlighted in yellow while those common in two are highlighted in purple. The rest are unique to their respective clusters. Class ratios are depicted under cluster sizes.

$ C_1 = 1856$ 6.25 : 2.07 : 1	$ C_2 = 2845$ 1.27 : 1.15 : 1	$ C_3 = 2049$ 1 : 1.14 : 3.07
WBC_last	HCT_last	SysABP_first
SOFA	BUN_first	GCS_last
HCT_first	PaO2_last	Age
Platelets_first	Creatinine_first	PaO2_last
Na_last	NIMAP_lowest	Glucose_last
HR_highest	MechVentDuration	HR_last
HR_lowest	Glucose_highest	Na_first
NISysABP_highest	GCS_highest	PaCO2_first
PaO2_last	HR_lowest	DiasABP_lowest
PaO2_first	Glucose_last	Weight

score of 0.495 while the student model trained on the prediction scores of DEEPCAC attains an AUPRC of 0.358 (both evaluated on the same training and test datasets). C_3 has a majority of patients who spend a large time in the ICU while C_1 ’s majority population spent a relatively small time in the ICU. In Table 7 we report the features that are most significant across the 3 clusters (determined using p-values). This indicates that the three clusters are most directly distinguished by the Mechanical Ventilation parameters and the UrineOutput. But within those clusters, the patient LoS depends on variables presented in Table 8. We can cluster the dataset with any other variable also (say Age) and thus discover how LoS depends on different variables for various

age groups.

Table 9: AUC Scores for Time series datasets. Row-wise best result in bold. $*p < 0.05$, $**p < 0.01$ indicates significantly better performance of DEEPCAC-TS compared to the baseline.

AUC		ACTPC-TS	GRASP-TS	DEEPCAC-TS
ARDS-TS	2	-	0.493	0.615**
ARDS-TS	3	-	0.519	0.605*
ARDS-TS	4	-	0.505	0.565*
Sepsis-TS	2	-	0.491	0.76**
Sepsis-TS	3	-	0.528	0.769*
Sepsis-TS	4	-	0.465	0.752**

15 DEEPCAC-TS

We extend DEEPCAC, ACTPC and GRASP to handle time series data by replacing the Stacked Autoencoder with LSTM based autoencoder. α and β for DEEPCAC-TS are set to 20 and 5 respectively. For GRASP and ACTPC, we use the hyperparameters recommended in their original papers.

We evaluate all algorithms on the ARDS and Sepsis datasets as mentioned in table 1. We use the first 24 hours of data to predict risk (of each condition, separately) in the remaining ICU stay, which is aligned with a hospital-centric schedule for prediction. Risk prediction is formulated as a binary classification problem. The prediction task is to predict whether a patient will develop the condition at point in time after the 24 hours of stay in the ICU. All patients whose length of ICU stay is < 24 hours and those who develop the condition within 24 hours of their ICU stay are excluded.

The AUC and AUPRC scores are mentioned in tables 9 and 3. We note that DEEPCAC-TS performs better than GRASP for both the datasets and for all $k = 2, 3, 4$. ACTPC-TS did not finish in time for both the datasets. All results are 3-fold averaged over the test dataset. The AUC and AUPRC scores for DEEPCAC-TS are better than those obtained by DEEPCAC on the static ARDS and Sepsis datasets as expected.